A CASE STUDY OF THREE DIMENSIONAL INVERSIONS OF ELECTRICAL RESISTIVITY TO IMAGE GEOTHERMAL SYSTEM IN KOROSI GEOTHERMAL PROSPECT-KENYA

Eng. Mathew Muthuuri Arthur

A Thesis Report Submitted in Partial Fulfilment for the Award of the Degree of Master of Science in Geothermal Energy Technology in Geothermal Training and Research Institute, Dedan Kimathi University of Technology.

March, 2018

DECLARATION

I affirm that the work on this report is my original exertion to the best of my knowledge.

Mathew Muthuuri Arthur

Sign: …… **Date:** ……

G296-03-020/2013

Supervisors' declaration:

We confirm that the work reported in this thesis was carried out by the candidate under our supervision as University supervisors

Signature: ……..Date: ……...

Professor Nicholas Mariita

Department: ……...

Institution: ……..

Sign: …….....**Date:** ……..

Doctor Fukuoka Koichiro

Department: ……...

Institution: …….

DEDICATION

I dedicate this work to my beloved father Arthur Ndumba who passed away during the course of my studies, for his encouragement to be the best I could in life and impressing on me the importance of education at my tender age.

ACKNOWLEDGEMENT

I wish to acknowledge GDC for purchasing a high end, high speed computer that made this research possible. The author also wishes to acknowledge the following; Honda Mitsuru, Deputy Manager West Japan Engineering Consultants Inc, Dr. Fukuoka Koichiro, West Japan Engineering Consultants Inc, Prof. Mariita Nicholas, Director GeTRI for untiring support and guidance on this research.

My sincere gratitude also goes to my wife for her unfathomable support heretofore.

I cannot forget my allies in DeKUT University at large. Cheers!

GOD BLESS YOU ALL!!

Table of Contents

List of figures

Abbreviations and Acronyms

1D	One dimension
2D	Two dimension
3D	Three dimension
EDI	Electrical data interchange files
EM	Electromagnetic
Rx	Receiver coil
Tx	Transmitter coil
Emf	Electro motive force
E_x	Electric field in North-South direction
E_y	Electric filed in East-West direction
GDC	Geothermal Development Company
H_x	Magnetic field in the North - South direction
H_y	Magnetic field in the East - West direction
H_z	Magnetic field in the vertical direction
MT	Magneto-Telluric
NLCG	Nonlinear conjugate gradients
REBOCC	Reduced basic OCCAM inversion
RRI	Rapid relaxation inversion
SSMT2000	Raw data robust processing software
TE	Transverse electric
TEM	Transient electromagnetic
TM	Transverse Magnetic
TE	Transverse Electric
WinGlink	2-D inversion program
WSINV3DMT	3-D inversion program

ABSTRACT

In real situation the physical earth is in three Dimension (3D), a two dimension (2D) and one dimension (1D) earth models may not therefore explicitly explain or characterize the 3-D Earth in all situations. This is a simple and apparent reason why one needs a higher dimensional interpretation of Magnetotelluric (MT) resistivity data in modelling geothermal reservoirs. 2D MT interpretation is frequently applied in geothermal assessment and in many cases has effectively provided accurate information of geothermal reservoirs. Conversely, due to intricate geological environments, 2D interpretation sometimes fails to produce representative models, especially for deeper parts of reservoir. It is also the case in other natural resource assessment and geo-scientific research, such as oil exploration or underground water resources, volcanological studies etc. In this regard, 3D interpretation techniques are now in high demanded for understanding of true resistivity structures in various geological applications. This research describes (3D) MT inversion for 147 MT data sets obtained from Korosi geothermal prospect. The inversion scheme was based on the linearized least-squares method with smoothness regularization. Forward modelling was done by the finite difference method, and the sensitivity matrix was calculated using the adjoint equation method at each iteration. The research has helped to recover deeper resistivity structures in Korosi geothermal prospect. The results further infer two geothermal reservoirs below Korosi - Chepchuk massif. A close correlation between major surface structures, fumaroles, and the 3D model is observed. Consequently, the extent of geothermal resource at Korosi - Chepchok prospect, the depth of the inferred geothermal reservoirs. This research will in future assist in future prospecting of Korosi Geothermal area.

CHAPTER ONE

1. INTRODUCTION

1.1. Background of the study

Processing of joint Magnetotelluric (MT) and Transient Electromagnetic (TEM) one dimensional inversions recovers a resistivity model varying with vertical axis of the earth only thus ISO resistivity maps and cross-sections are produced. In Two dimension inversion of resistivity cross sections, conductivity is assumed to change with vertical axis of the earth and in one other direction and being constant in the other rectangular horizontal direction. Much data has been processed and explained by use of Transverse Electric (TE), Transverse Magnetic (TM) and both TE+TM with the objective of assessing which of the approaches results to a resistivity structure that is more precise. Transverse Electric approach describe current flowing in the same direction as strike (Parallel) whereas Transverse Magnetic approach usually describes current flowing perpendicular to the structure. Computer Technology and programming skills developments have made 3D inversion of MT data possible. In actual sense earth is 3-dimensional where electrical conductivity changes in every other direction; σ(x, y, and z). Therefore, the 3D inversion of MT off-diagonal impedance elements has been performed in this research resulting in more consistent and comprehensive results than has been attained in the same geothermal prospect. It is in this perspective that resistivity data was acquired and subjected to 3D inversion to image geothermal system in Korosi geothermal prospect.

1.2 Geographical area of Research

Korosi geothermal prospect is located in the northern segment of Kenya's rift valley. It is located within latitudes 0^0 40' N and 0^0 53'N and longitudes 36^0 00' and 36^0 13' within the rift graben. Korosi geology to a large extent has intermediary lavas mainly trachytes and trachy-andesite (Figure 1-2), which appear on the eastern and central parts of Korosi area, basalts which are dominant in the north, south and western areas. Nevertheless, fluvial and alluvial deposits dominate south western plains while plains in the western part are dominated by resistive overburden of air fall Pumice (Silas M. Simiyu, April 2010). Several methods have been used in this area to delineate the extent of geothermal resource. The commonest method employed in exploration for geothermal energy was electrical conductivity technique.

Figure 1-1: Map of Kenya geothermal resources areas with inset Korosi geothermal prospect.Source: Arthur M. M., 2016

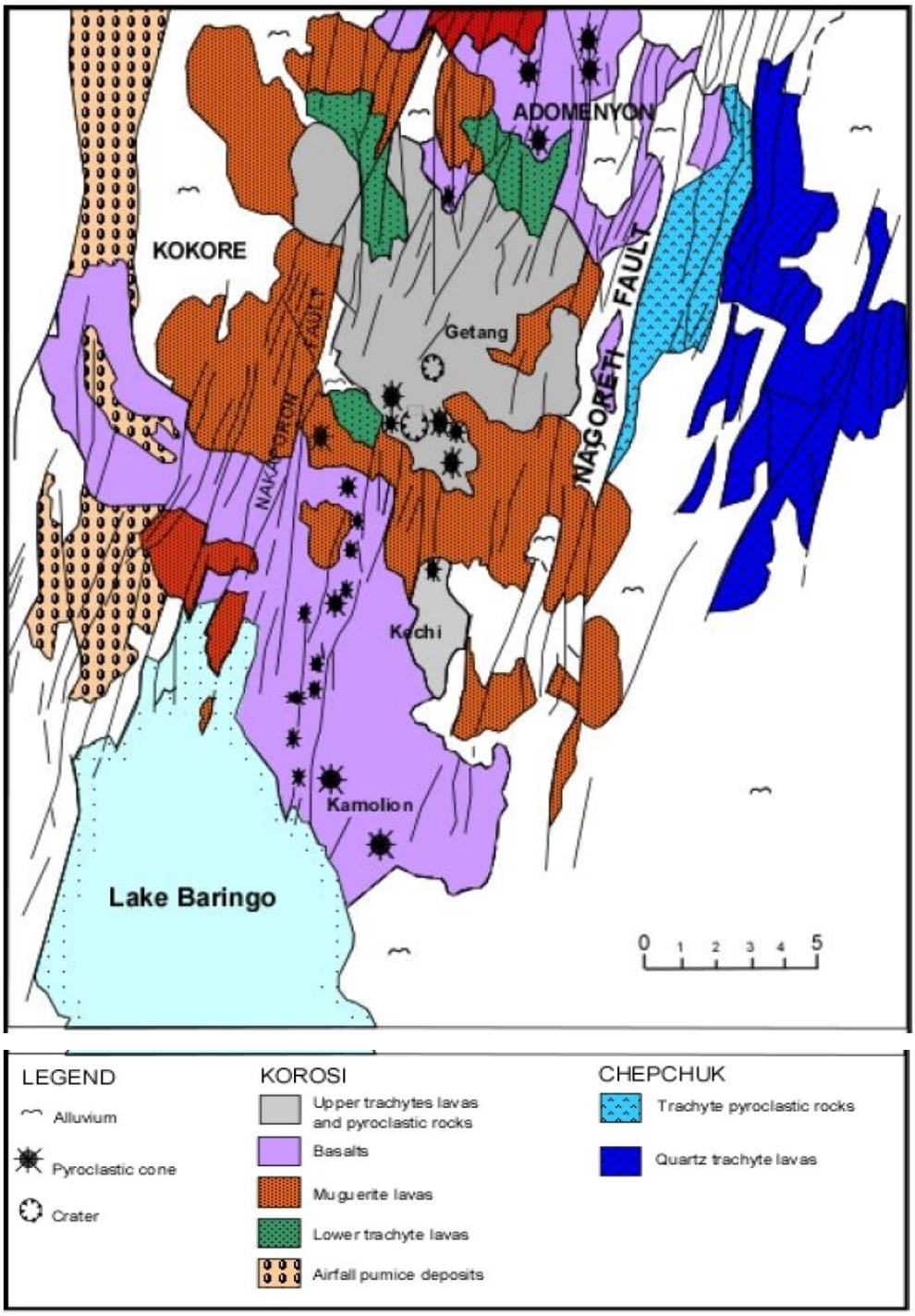

Figure 1-2: A map showing geology of Korosi - Chepchuk area. Source: Silas M. Simiyu, April 2010

Problem environment

The Earth is multidimensional, a 2D and 1D Earth models may not be appropriate to explain or represent the earth. Two-dimensional (2D) interpretations are now commonly applied to MT sounding data in geothermal investigations and has positively provided resistivity information of geothermal reservoirs especially at shallow depths. Nevertheless, due to intricate environments of geology, 2D interpretation occasionally does not yield models that are realistic, especially for deeper parts of reservoir (Uchida et. al 2001).

Results of 2D inversions has been a typical method for interpretation of MT data in the past few years. 2D inversion has delivered resistivity models in various geothermal fields and prospects thus making understood the resistivity features of geothermal reservoirs. In a 2D situation, data are more sensitive to anomalies that are deep and conductive in Transverse Electric (TE) than Transverse Magnetic (TM) modes. However, for TE-mode data, good fit usually cannot be achieved by a 2D inversion of MT data except where the structure of subsurface is 2D or almost 2D. Conversely, in a 2D inversion a fairly good fit could be achieved easily on a TM-mode data even for a structure that is three dimensional. This is why 2D inversion frequently utilizes only TM-mode data in geothermal surveys. Nevertheless, even if there is a small misfit in the TM-mode data, the recovered 2D resistivity model may not be realistic and also may include anomalies that are false. Particularly, the distribution of resistivity in the deeper parts of the reservoir is often not clear. These circumstances demonstrates the drawback of 2D interpretation of MT data for use in geothermal exploration. (Toshihiro Uchida* & Yutaka Sasaki, 2001)

Overcoming these problems, MT 3D inversion techniques have been intensively studied (e.g., Sasaki, 1999; Newman and Alumbaugh, 2000; Zhdanov et al., 2000; Mackie et al., 2001).

This research seeks to expand the limitations of Lower dimensional interpretation with respect to clarity and true representation of resistivity models. A higher dimensional data inversion and interpretation approach is a vital consideration to map geothermal system with more lucidity.

1.3 Statement of the problem

Improving the quality of lower dimensional electrical resistivity data 2D inversion to recover a representative model of the multi-dimensional earth.

1.4 Purpose of this Study

The purpose of this study was to delineate the geothermal resources using 3 dimensional inversion approaches. The higher the possible dimensional inversion of resistivity data, the closer to reality are the resulting resistivity structures. This was intended to improve resolution of the 1D resistivity structure in reference to geothermal system.

1.5 Objectives of this research

The main objective of this research was to interpret the general resistivity structure and analyse the extent of geothermal potential using 3 dimensional inversions of Magnetotelluric (MT) resistivity data derived from Korosi Geothermal Prospect to assist in future prospecting for geothermal resources.

Specific objectives of this research were;

- To achieve 3D resistivity model for the prospect.
- To define the depth of the geothermal reservoir.
- To compare and relate 3D resistivity model with surface geothermal manifestations and geological structures.

1.6 Research questions

- What was the average depth of the reservoir in Korosi Geothermal Prospect?
- What was the extent of the geothermal resource in Korosi Geothermal Prospect?
- Which were the possible drill sites for geothermal development according to electrical survey methods?

1.7 Justification for the Study

Unequivocally, earth is 3D thus a 2D and 1D earth models may not explicitly explain the 3D Earth. This is a simple and obvious reason why one needs 3D inversion of MT data to image geothermal systems. Consequently, sophisticated 3D techniques are highly needed to explain true structures of resistivity for different applications. Without correct models, there is a risk of inaccurate interpretations leading to an unattractive investment. A correlation of 1D, 2D and 3D has been done at Glass Mountain (Figure 1-3), from the result it is indicate that a lower

dimensional inversion of MT could lead to a somewhat wrong interpretation of the subsurface. A good relation is seen between 1D and 3D inversion results at shallow depths but a 2D inversion result seems to exhibit a different inference of the subsurface.

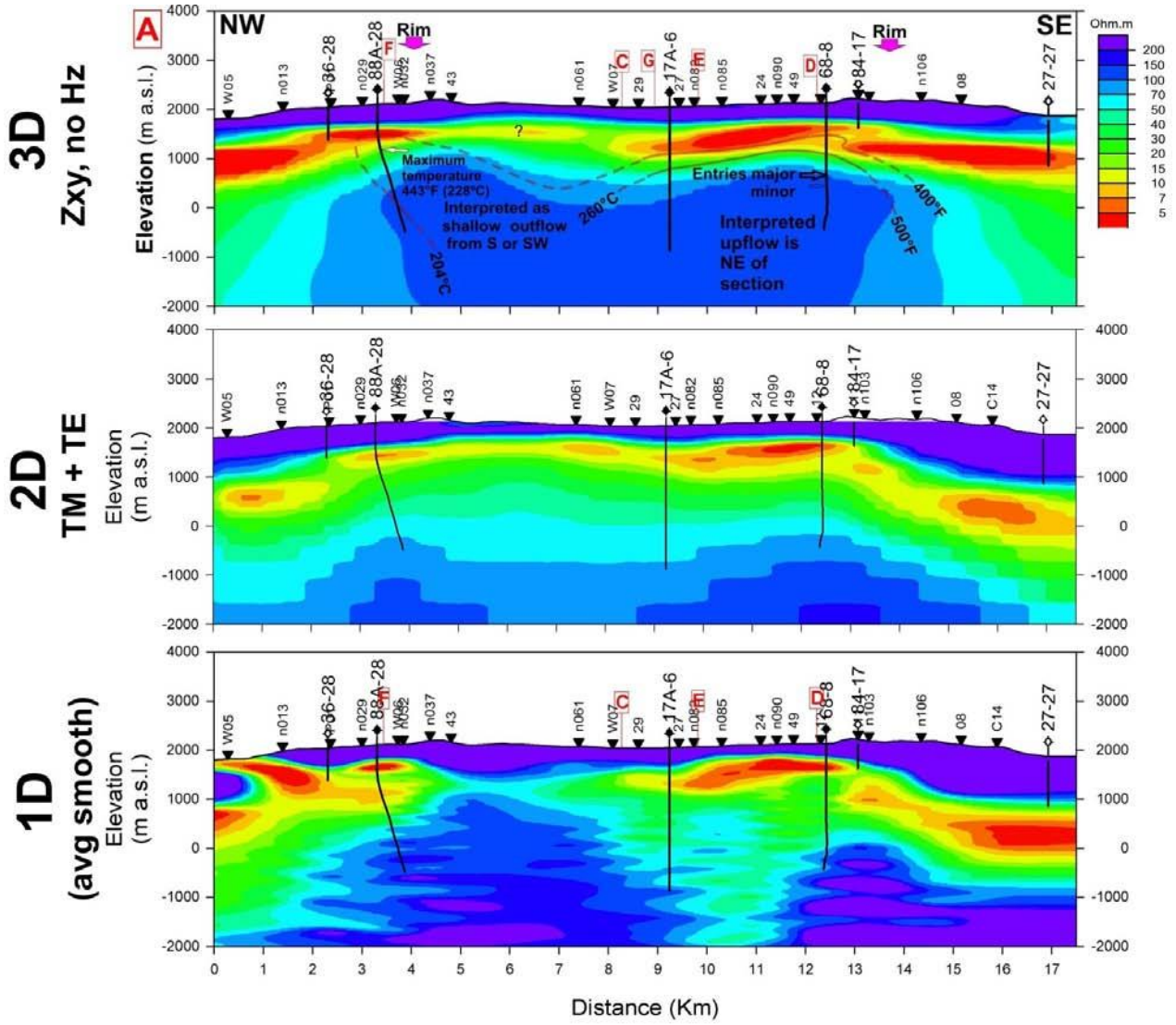

Figure 1-3: Cross-section with 1D, 2D and 3D MT resistivity inversions, wells, isotherms and MT stations. Source: Cumming, 2013

1.8 Delimitations of the study

Resistivity data has been collected since 2006 by different companies in the Korosi geothermal prospect. 161 No. MT soundings and 148 No. TEM soundings have been done at Korosi geothermal area. Data that was collected earlier and that which existed has been incorporated in this research. A very high speed computer with min of 64GB RAM and 3.0 GHz 16 cores is required. The computer is available in GDC and was used as a very important tool that facilitated feasibility of inversion of MT resistivity data in this research.

1.9 Limitations of the study

1.9.1 MT static shift problem

This is a method based limitations. Static shift in MT is a phenomenon that arises due to local surface or near-surface conductivity contrasts which change the electric field in direction and magnitude. Static shifts occur when the dimensions of anomalous body are much less than the skin depth. Nearly all electrical methods which probe the electric field on the surface of the earth are susceptible to static shift issues. This is prompted by the buildup of electric charges at resistivity boundaries making the electrical field to be sporadic close to these boundaries. Voltage and current distortion (current channeling), are responsible for producing static shift (Árnason, 2010). The static shifted data is expressed by an unknown factor (shifted on log scale) that scales the apparent resistivity, such that the apparent resistivity curves plot parallel to their real level. The shift is independent of frequency (Jones A. , 1988:) and does not affect the phase curve.

It is not feasible to identify static shift factor S, from an MT data that is recorded at a one site only. An indicator that static shift is present in the data is when a parallel shift between two polarizations of apparent resistivity curves occur. True curves of apparent resistivity may lie between, below or above the measured responses. The result of the shifts in the curves is a large errors in the inverted data; for example a shift where S = 0.1 results in tens of times as low resistivity value and about triple as small depths to boundary of resistivity (Árnason, 2008). In a volcanic environments where near surface conductivity variations are usually extreme, two dimension and three dimension models may contain untrue structures if correction of static shifts is not done. Static shift multiplier of less than 1 result in lower resistivity and reduced depth to boundaries whereas a multiplier more than 1 effects in higher resistivity and more depth to boundaries. Consequently, curves of MT data shifts downwards when measuring over conductive bodies and shifted upwards when measuring directly over surficial resistive bodies. Several methods that have been developed to solve static shift problem in MT. It has been claimed that the static shift problem can be dealt with by resolving the shallow resistivity structure around the dipole by measuring at high enough frequencies. This would be true if the earth was a pure Ohmic conductor, but in reality both capacitive and inductive effects are at play. Ogawa and Uchida (1996) and DeGroot-Hedlin (1991) have suggested using inversion algorithm on MT data to correct for static shift, the algorithm assumes that

shift multipliers is stochastic and that the product of the shift multipliers is near unity for several data points. Another way and the one that has been used in this report is the use of TEM method with a Central loop-induction configuration to fix static shift problem on MT soundings. This fact owes to the idea that, in transient electromagnetic (TEM) measurements at late time there are no distortions due to near surface in-homogeneities as TEM does not measure electric field. The method has been tested by calculations (e.g. Sternberg et al., 1988, (Árnason K., 2008) and proved to be a useful method to correct for the shifts problem in MT soundings. It must therefore be born in mind that successful interpretation of MT data depends significantly on reliability of the correction of static shift. Causes of static shift in MT measurements as suggested by Jiracek (1990), are described below.

1.9.2 Current distortion

Telluric currents flowing in subsurface of the earth encounters resistivity anomalies that affect its path of flow. Whether the conductivity anomaly is high or low determines how the current is transmitted. Currents usually take a low resistance channel thus higher conductivity anomaly causes higher currents to transmit and low currents to transmit in lower conductivity anomaly. As a result of primary electric field, charges accumulate on the boundaries of these anomalous conductivity depending on the conductivity of the anomalous area relative to its surrounding environment. In a region that is resistive, the positive charges accumulate on the side that face the primary electric field, inducing a secondary electric field in and around the anomalous conductivity thus lateral flow-around effect. The secondary field is in the direction of the primary field within the resistive body. (Figure 1-4a). In an anomalous conductive area, a negative charges build-up arises on the side facing the primary electric field, inducing a second electric field that is opposing the primary field due to lateral current gathering effect (Figure 1-4b). The distribution of second electric field exterior to the anomalous area is dependent on the configuration of the primary fields producing it.

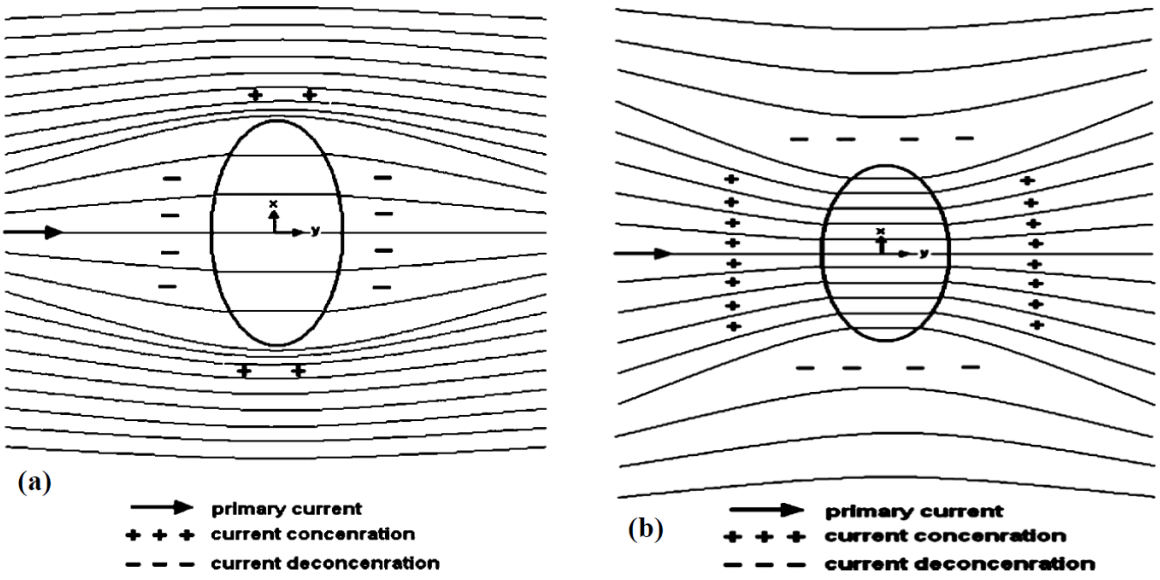

Figure 1-4: Current channeling due to an inhomogeneous conductivity showing: a) Current Flowing around a resistive anomaly and b) Current channeling through effect in a conductive anomaly. Source: Lichoro, 2013

Charge distributions that build up on the shallow body surfaces causes galvanic distortions, which result to electromagnetic field that is anomalous. This magnetic field that is anomalous is small, while the electric field that is anomalous is of the same order of magnitude as its local counterpart and is not frequency dependent (Bahr, 1988); (Jiracek, 1990) Thus, galvanic distortion is treated as the existence of an electric field that is anomalous. (Zhang, 1987); (Bahr, 1988).

1.9.3 Topographic effects

Uneven or bumpy topography may yield static distortions where the currents are concentrated underneath depressions and dispersed below peaks leading to electric field which increases in valleys and reduces on hills owing to the galvanic effects. Hence, the current density and the associated MT field are high in a basin and low on hilly area. This presents an apparent shift of a resistivity curve shift up or down which can be treated as static shift. Shift correction by TEM can considerably account for the topographical effects (Figure 1- 5).

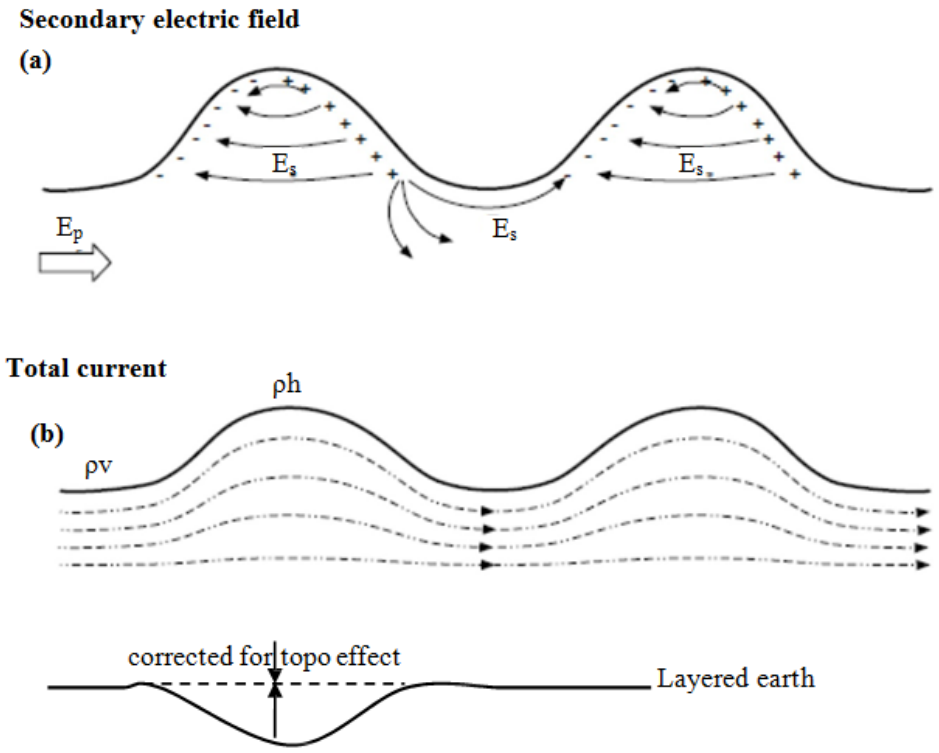

Figure 1-5: Total current distribution and secondary electric field due to topography and correction for the topographical effect. Source: Lichoro, 2013

1.9.4 Run time and hardware limitations

The use of 3D inversion modelling of MT data for geothermal system is a promising technique to obtain reliable high resolution resistivity images of geothermal structures in the system. However, obtaining a resistivity model from a 3D inversion is a complex and computationally demanding task.

Obtaining a higher resolution resistivity model using 3D inversion of MT data has high computational cost, both in internal memory required and CPU run time. The total cells number in the model, the number of discrete frequencies selected, and the setup of the inversion have great importance in terms of memory and CPU requirements.

There two main matrices need to be stored in memory N x M Sensitivity matrix (**J**) and N x N Representer matrix ($\mathbf{JC_dJ^T}$). Any time one would want to undertake a 3D inversion, analysis on whether or not the RAM is enough is done. This poses a challenge where the RAM requirement is less that the available according to RAM (bytes) = $1.2 \times (8N^2 + 8NM)$, where N and M are number of stations and model size respectively.

1.10 Assumptions of this study

This study assumed that the data available was of high quality and had most if not all apparent resistivity curves in 3D as revealed by polar curves of just a few soundings. This study further assumed that impendence elements Zxx and Zyy are zero or near zero.

1.11 Chapter one summary

The earth is multidimensional, an approach to resistivity modelling using a higher dimensional inversion of resistivity data is a worthy course. This is necessitated by the justification of this study which states that there could be loss of investment if the accuracy of the data inversion is not observed. The purpose of this study is to seek a clearer resistivity structure. The limitations of this method can be overcome as sited in the delimitation of this study thus making the research feasible.

CHAPTER TWO

2.0 LITERATURE REVIEW

2.1 Introduction

Our country Kenya is gifted with huge geothermal resources which lies in the Kenyan Rift system that divides the country longitudinally from south to north. Preliminary explorations revealed that geothermal potentials in Kenya exceed 7,000 MW_e and are in excess of Kenya's electricity demand over the next 20 years period. Out of this electricity potential low power is being utilized for other uses directly and indirectly. Geothermal Development Company (GDC), Kenya Electricity Generating Company (KenGen) in partnership with the Ministry of Energy (MoE) commenced detailed surface studies for most geothermal prospects in the Kenya rift, which include Suswa, Longonot, Menengai, Lakes Bogoria, Korosi Olkaria, Eburru, Baringo and Paka.

The Least Cost Power Development Plan (2008-2028) prepared by the Kenyan Government indicated that geothermal power plants have the lowest unit cost of electricity and thus appropriate for base load and hence, endorsed for additional geothermal development. In 2009 electric power demand in Kenya stood in excess of 8% annually (Silas M. Simiyu, 25-29 April 2010). To counteract growing electricity demand, the Kenya Government has ventured in an ambitious generation expansion plan to install additional electric power by the year 2019 and 2030 from geothermal resources respectively.

Geophysical studies in known geothermal areas of the bedrock resistivity, at depth, is influenced by the relative position of the water table, salinity, acid surface leaching (ground alteration) and underground temperature. High resistivity values are predominant at the surface within lava fields except in regions affected by superficial acid leaching. Often, low resistivity (<10 Ω-m) layers at shallow depths do correlate with geothermal features, with deeper higher resistivity inferring high temperature geothermal systems. (Arthur, 2016)

This chapter contains the previous works done on Korosi Geothermal Prospect by different researchers and their findings. Maps of data coverage progress from 2006 to current are shown. The essence of higher dimensional inversion of MT data is explicit by virtue of previous results based on 1D inversion.

2.1 Review of theory and principles of electrical methods

2.1.1 Electrical methods

Electromagnetic techniques have proved a useful tool in geophysical geothermal investigations. This is because the distribution of resistivity in geothermal dominated areas is not determined by the host rock distribution only, but is also related directly to the circulation of geothermal fluids, hydrothermal alteration minerals etc.

2.1.2 Transient Electromagnetic (TEM) Method

TEM method comprises of transmitting a current of constant level through a wire loop thus building a magnetic field that is constant and of known strength (Figure 2-1). The current is interrupted abruptly by turning off the current transmitter thus inducing, in according to Faraday's law, a short period voltage pulse in the ground, which causes a loop of current to flow in the close locale of the transmitter wire (Figure 2-1). After the transmitter's current is interrupted, the current loop can be thought of, as an image in the ground of the transmitter loop (see Figure 2-1). However, due to heat loss in the ground, the amplitude of the current starts to decay tending to zero immediately. This decaying current correspondingly induces a voltage that causes more current to flow, but now at a larger distance from the transmitter loop, and also at greater depth and the induction cycles continues. This current that flow deeper also decays due to ground resistance thereby inducing deeper current flow.

The penetration depth of the transient electromagnetic sounding current depends on the length of time the electromagnetic induction in the Rx coil can be traced before it decays to noise level. At a later time, the induced e.m.f (Volts) in the Rx coil in a half space that is homogeneous and of conductivity, σ is;

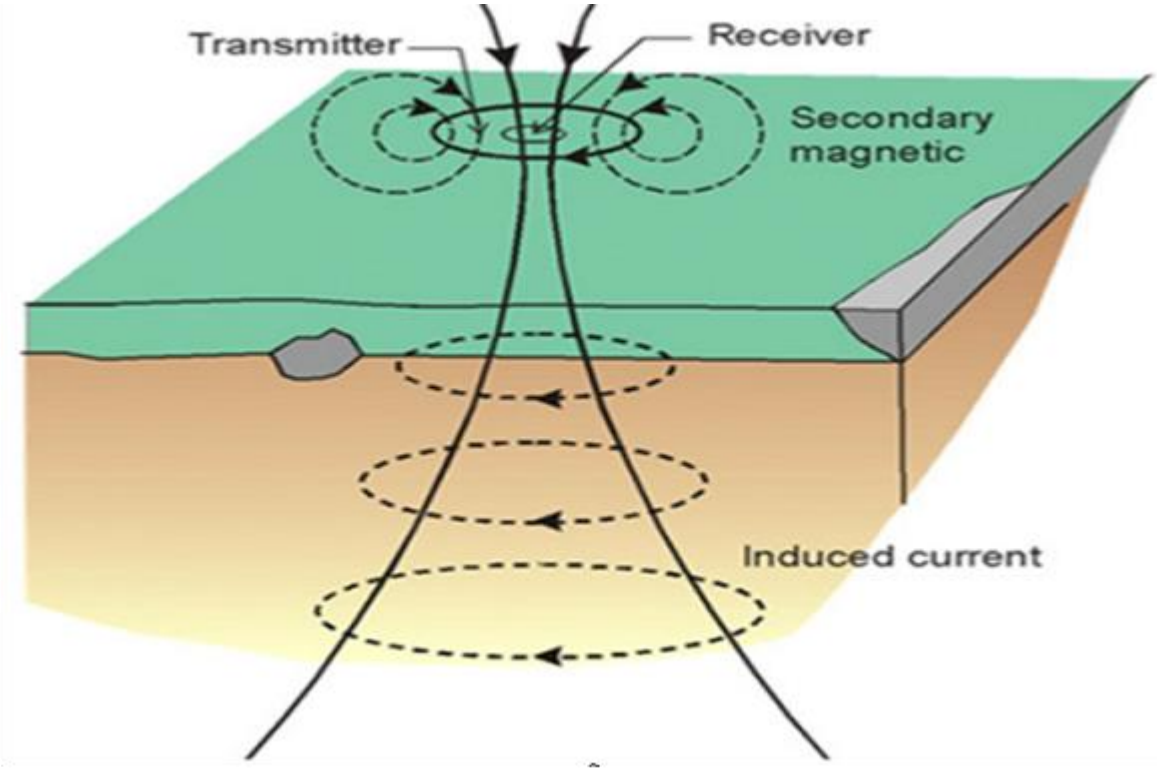

Figure 2-1: The central wire loop configuration for TEM method presenting how current flows in the environs of the Tx loop.Source Hersir, 1991.

$$V(t, r) \approx I_0 \frac{C(\mu_0 \sigma r^2)^{\frac{3}{2}}}{10\pi^{\frac{1}{2}} t^{\frac{5}{2}}} \quad \text{(Árnason, 1989)} \tag{1}$$

Where $C = A_r n_r A_s n_s \frac{\mu_0}{2\pi r^3}$

And

t = Time that has elapsed after interrupting transmitter current (s);

A_r = Cross-sectional area (CSA) of the Rx loop (m^2);

μ_0 = Magnetic permeability (H/m);

A_s = Cross-sectional area (CSA) of the Tx loop (m^2);

n_r = No. of winding loops of the Rx;

n_s = No. of winding loops of the Tx;

I_0 = Tx wire loop Current (A);

r = Tx wire loop Radius (m);

$V(t, r)$ = Induced e.m.f Transient (V).

It can thus be proved that the transient e.m.f voltage for later time, with current in the Tx loop turned off abruptly, is proportionate to $\sigma^{3/2}$ and decays to noise level in a period $t^{-5/2}$. Later time apparent resistivity can thus be defined by resolving for ρ_a in Equation (1), leading to Equation (2): (Hersir, 1991) Note: Apparent resistivity ρ_a is the reciprocal to Conductivity σ.

$$\rho_a = \frac{\mu_0}{4\pi}\left[\frac{2I_0\mu_0 A_r A_s n_r n_s}{5t^{5/2}v(t,r)}\right]^{2/3} \quad (2)$$

2.1.3 Magneto-telluric (MT) method

MT is a passive electrical method for geophysical exploration used to investigate the subsurface conductivity structure. Naturally varying magnetic fields of the earth induces flowing currents in the earth subsurface with respect to the resistivity of the earth's subsurface. Magnetic fields (H_x, H_y, and H_z) and electric fields (E_x and E_y) are acquired and measured on the surface of the earth in two directions (Figure 2-2). (Gichira, 2012)

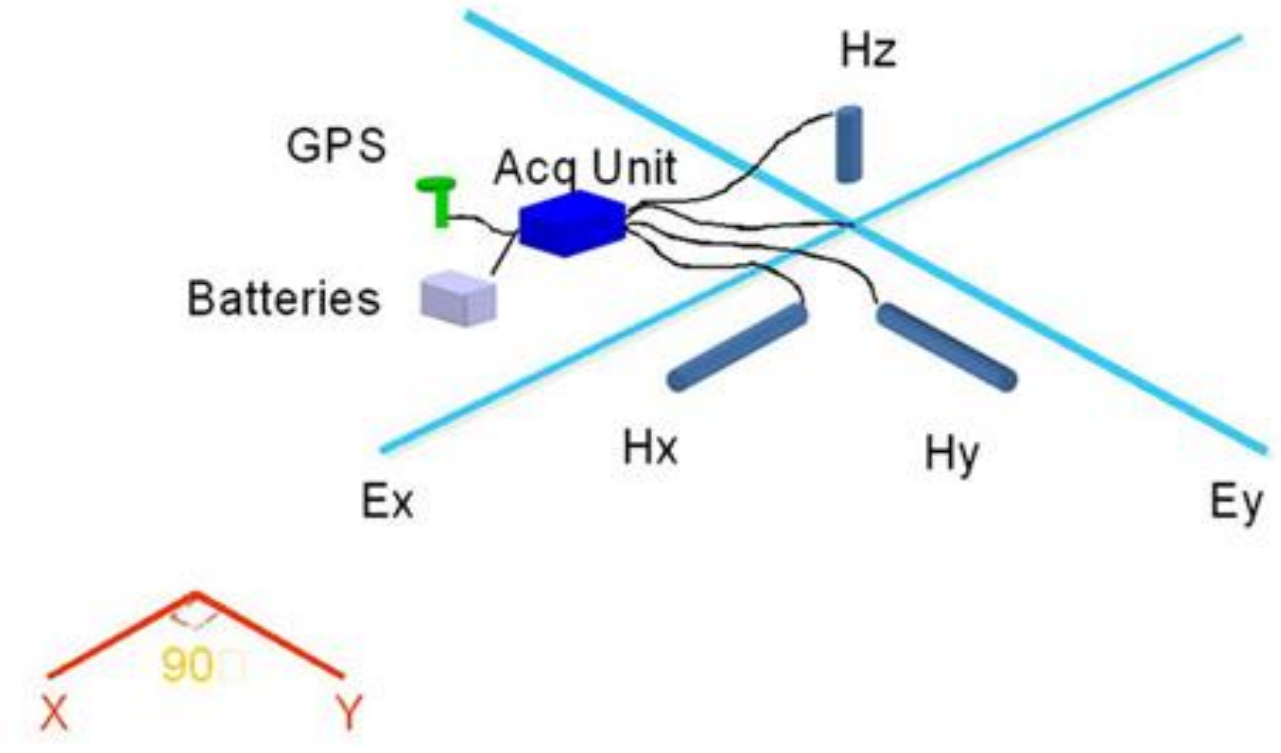

Figure 2-2: Five channel MT field setup. Source: Geophysics,Phoenix, 2005

Magnetic field and electric field at right angles are related by the impedance element thus apparent conductivity of the subsurface can be deduced. Information about the Resistivity of shallow depths are given by analysis of high frequency signals while analysis of low frequency signals are able to provide info about the conductivity at a deeper portion of the earth. Signals of frequencies that are low<1Hz have originate from the ionosphere and magnetosphere. Low frequency (<1Hz) signals are caused by interaction of solar wind (plasma) with magnetic field of the earth, while the high frequency >1Hz signals hails from lightning discharges near equatorial regions. The above natural phenomena produces signals on an entire frequency range of from a thousand seconds to 10 kHz (Gichira, 2012).

Review of previous works done on Korosi Geothermal Prospect using MT and TEM methods.A geophysical survey was done by the Ministry of Energy in the late 1980s using the vertical Schlumbeger configuration as part of a reconnaissance survey for the North Rift. Examinations of these few soundings indicate that their depth of penetration is not deep enough to determine the sizes and exact location of the anomalies accurately.

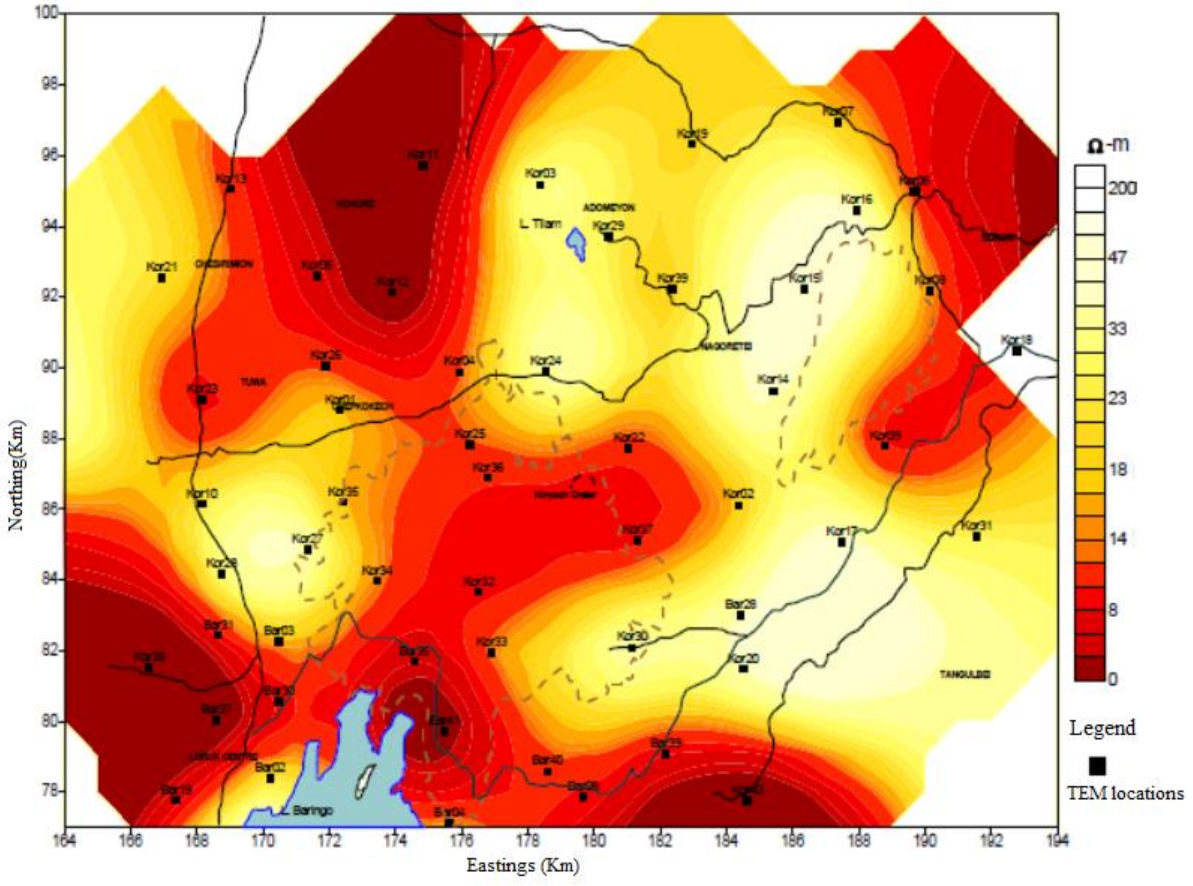

Figure 2-3: TEM station coverage (until 2006). Source: Mariita, 2006

The station density was about 1 station per 50 km^2 (Deflora, 2011). During interpretation of the data, since the station density was low and also since no additional information about homogeneity and isotropy or rocks at depth was available, no attempt was made to obtain resistivity vs. depth columns at each station. Re-evaluation of this data has indicated a complex resistivity pattern with depth of penetration not going very deep, less than 1000 m below surface in many cases.

In the year 2006 KenGen carried out both MT and TEM resistivity study of the Korosi prospect area. The coverage then is as shown in the Figure 2-4 below whereby only 36 MT and 44 soundings of TEM were carried out using one Phoenix MT equipment and Zonge TEM system.

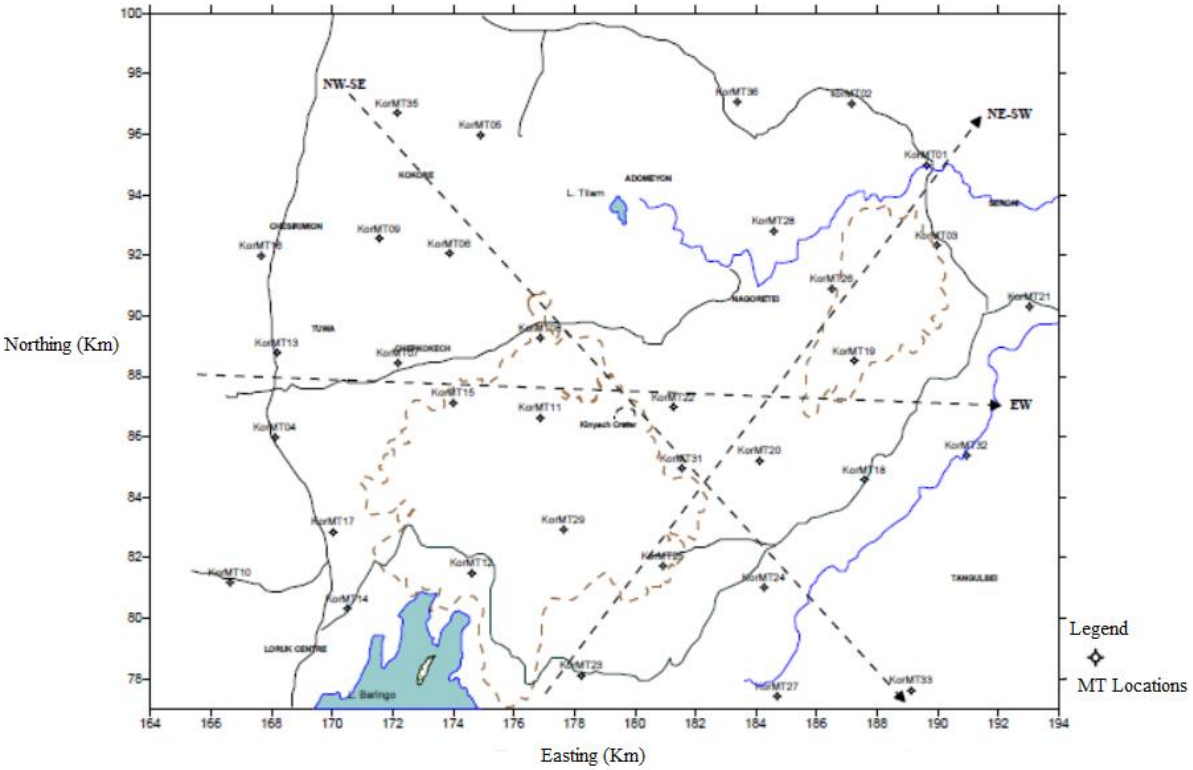

Figure 2-4: MT station coverage (Until 2006). Source: Mariita, 2006

From both MT and TEM areal coverage it was indicative that there was need to collect more resistivity data from this region, particularly MT in order to define the resistivity structure much clearly.

2.2 Results of work done until 2006

The results of the previous study indicate that there could be a geothermal resource in Korosi area possibly underneath Korosi volcano with estimated temperatures ranging about 300°C as deduced from gas geo-thermometry. Results of previous study indicate that Korosi has electric power potential of over 450 MWe (Simiyu, 2010). Three exploration wells (K-1, K-2 and K-3) were sited within the prospect as indicated in figure 2-5 below.

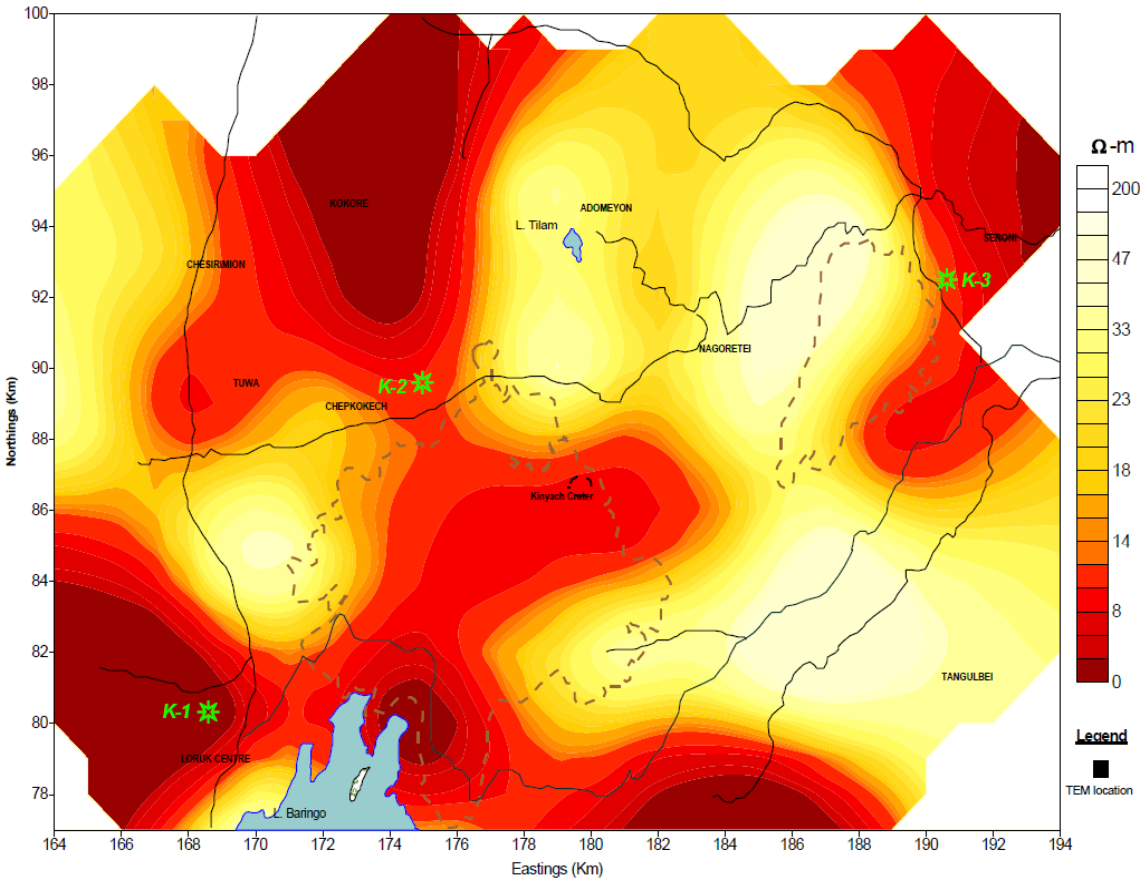

Figure 2-5: Exploration wells sited from the results of 2006 study. Source: Mariita, 2006.

2.3 Transient Electromagnetic (TEM)

TEM soundings were undertaken in Korosi-Chepchuk prospect area spread using Central Loop TEM Array. In all the soundings, a square wire loop of 300m x 300m to transmit current. Transmitting half-duty cycle square wave current was done at frequencies of 4 and 16 Hz. A Logarithmic spaced sampling gates were used with 16 Hz having 25 gates starting at 36.14µsec to 12.18msec; 4 Hz had 31 sampling gates starting at 36.14µsec to 48.42msec at every

repetition, some stacked repeated transients were moved to a Computer facility for processing and interpretation.

Raw data files were read and downloaded from the GDP-16 receiver by using TEM SHRED (a Zonge Engineering program) and the TEM-AVG (also a Zonge Geophysics program) was used to calculate standard deviations average and of repeated voltage transient measurements and later time apparent resistivity as a function of time. WinGlink (Geosystem) interpretation program was used to perform 1D inversion on the data. A total of 49 No. TEM soundings were done thus bringing the total to 93 No. soundings. (Muturia Lichoro, 2013)

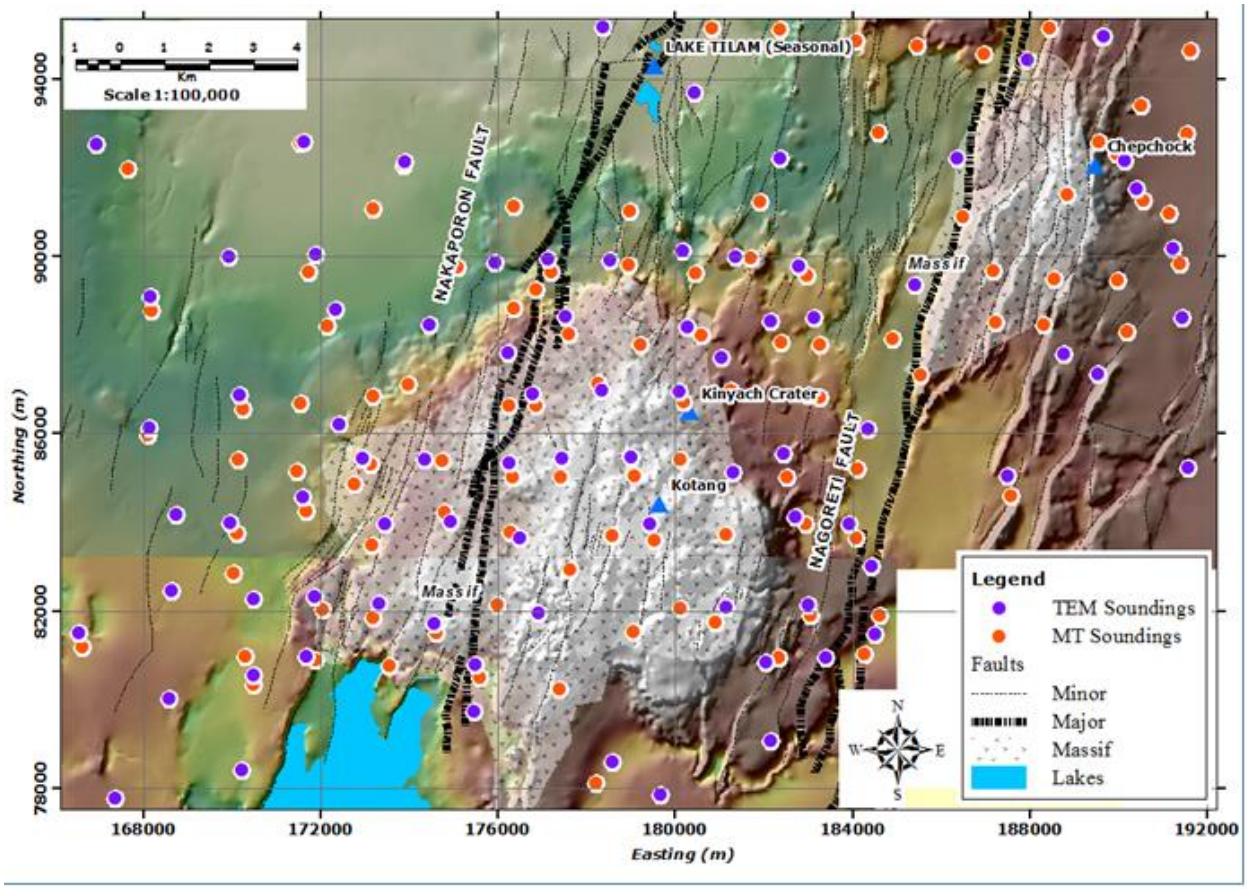

Figure 2-6: Current MT and TEM locations map (Until 2011). Source: Deflora, 2011

2.4 Magnetotellurics (MT)

MT soundings were carried in Korosi-Chepchuk prospect using MTU-5A data acquisition systems from Phoenix Geophysics, with each sounding taking an average period of 17 hours.

SSMT2000 was used to produce Fourier transformed data from the raw time-series, i.e., conversion from time domain to frequency domain after which MTU-Editor software was used to write the MT data files to standard *.edi format for use with the geo-systems' WinGLink

geophysical interpretation software to perform 1D inversion. EM data from GDP – 16 collected on same locations as the MT sites were also processed on WinGLink code, where 1D models produced were used for correcting static shift on the MT data. As show in figure 2-6 additional 73 No. data points were carried out thus making a total of 109 soundings (Lichoro, 2013.)

2.5 Results of work done until 2011.

2.5.1 ISO-resistivity maps

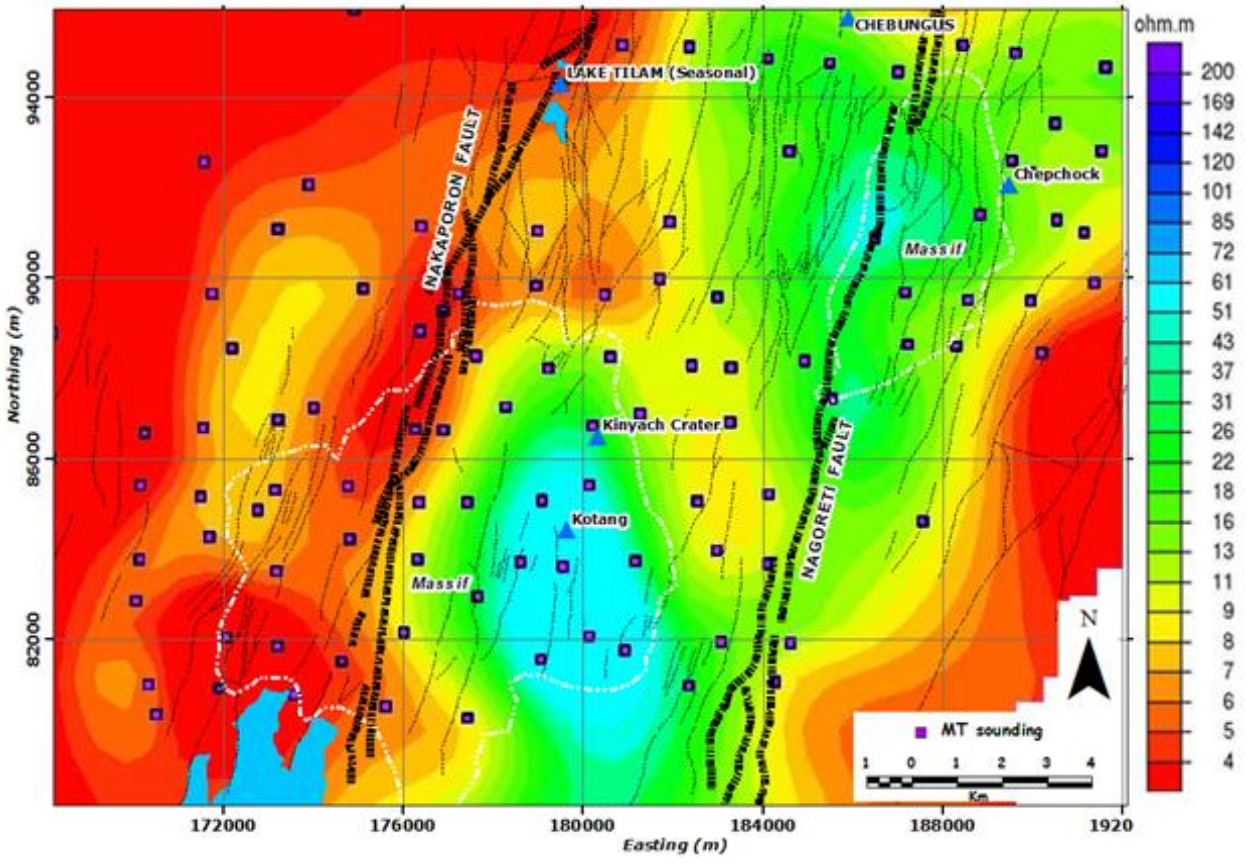

Figure 2-7: Resistivity at 500m above sea level. Source: Raymond, 2011

a) Resistivity at 500 meters above sea level (masl)

At shallow depths (500 m beneath the surface of earth) there are structure that have low resistivity (Figure 2-7) seen on the western part of the prospect due to low alteration clay minerals. Another patch is seen on the eastern part but not supported by enough data. On the north eastern part a fairly high resistivity is seen of about 26 Ohm.m which is caused by

unaltered formations and which seems to align on the direction of major structures in the prospect (NNE).

b) Resistivity at sea level

At sea level (Figure 2-8) hydrothermal alteration sets in on the Western part of this prospect area resulting from low temperature hydrothermal clay minerals such as smectite and illites and also on the North eastern parts which connects to the southern flanks of the Paka prospect to the North though the data is not enough to clearly define it Northwards. On the central part of the prospect a resistivity anomaly of less than 40 ohm.m is evident and this can be interpreted as the reservoir zone for this prospect area and is characterised by alteration minerals of high temperature such as chlorites and epidotes.

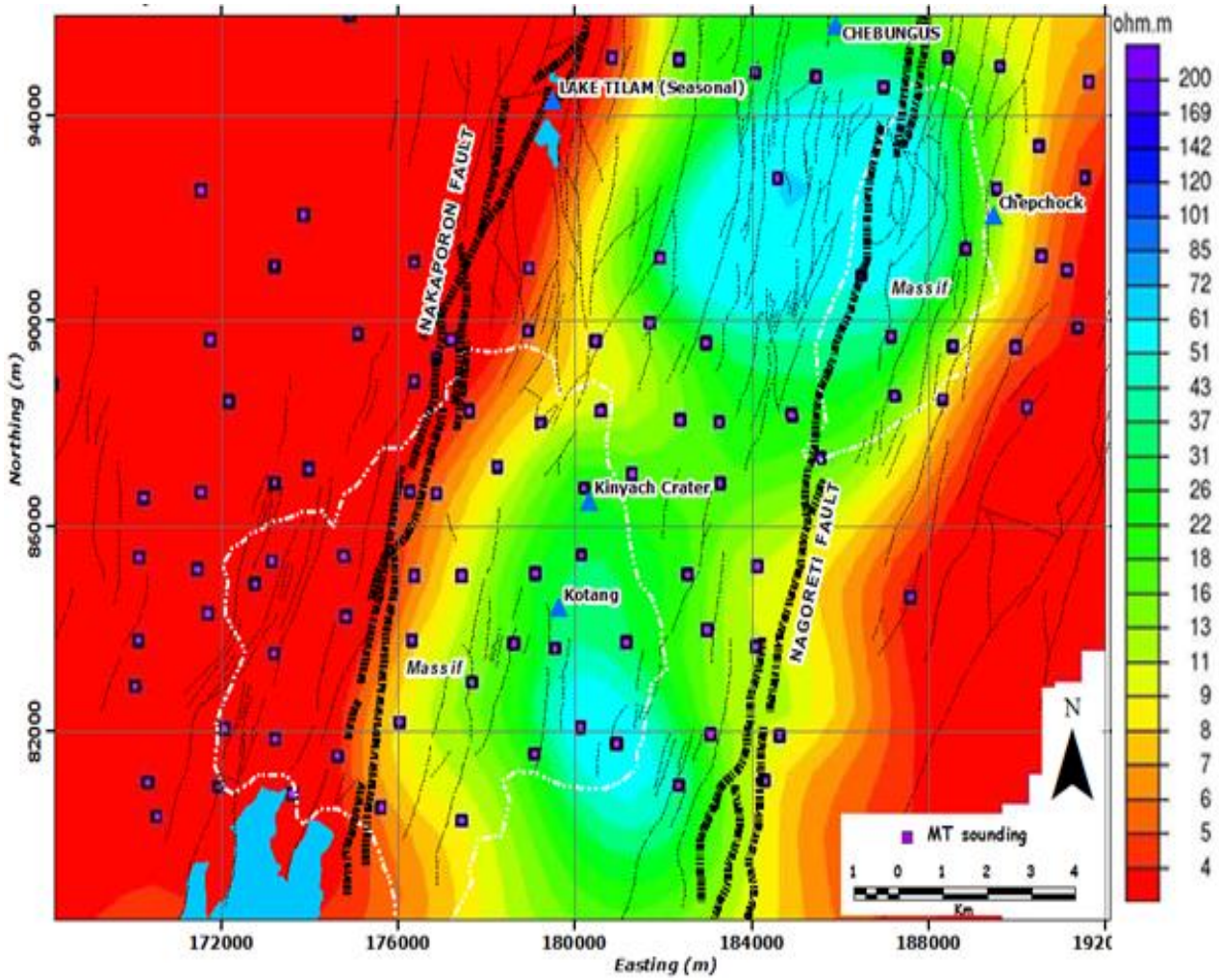

Figure 2-8: Resistivity at sea level. Source: Deflora, 2011

c) Resistivity at -1000 meters below sea level (mbsl)

At 1000 mbsl (Figure 2-9) which is still the reservoir zone a fairly high resistivity still exists an indication of high temperature minerals. A high resistivity anomaly aligns itself from Kinyach crater towards NE which is due to unaltered formations at this level.

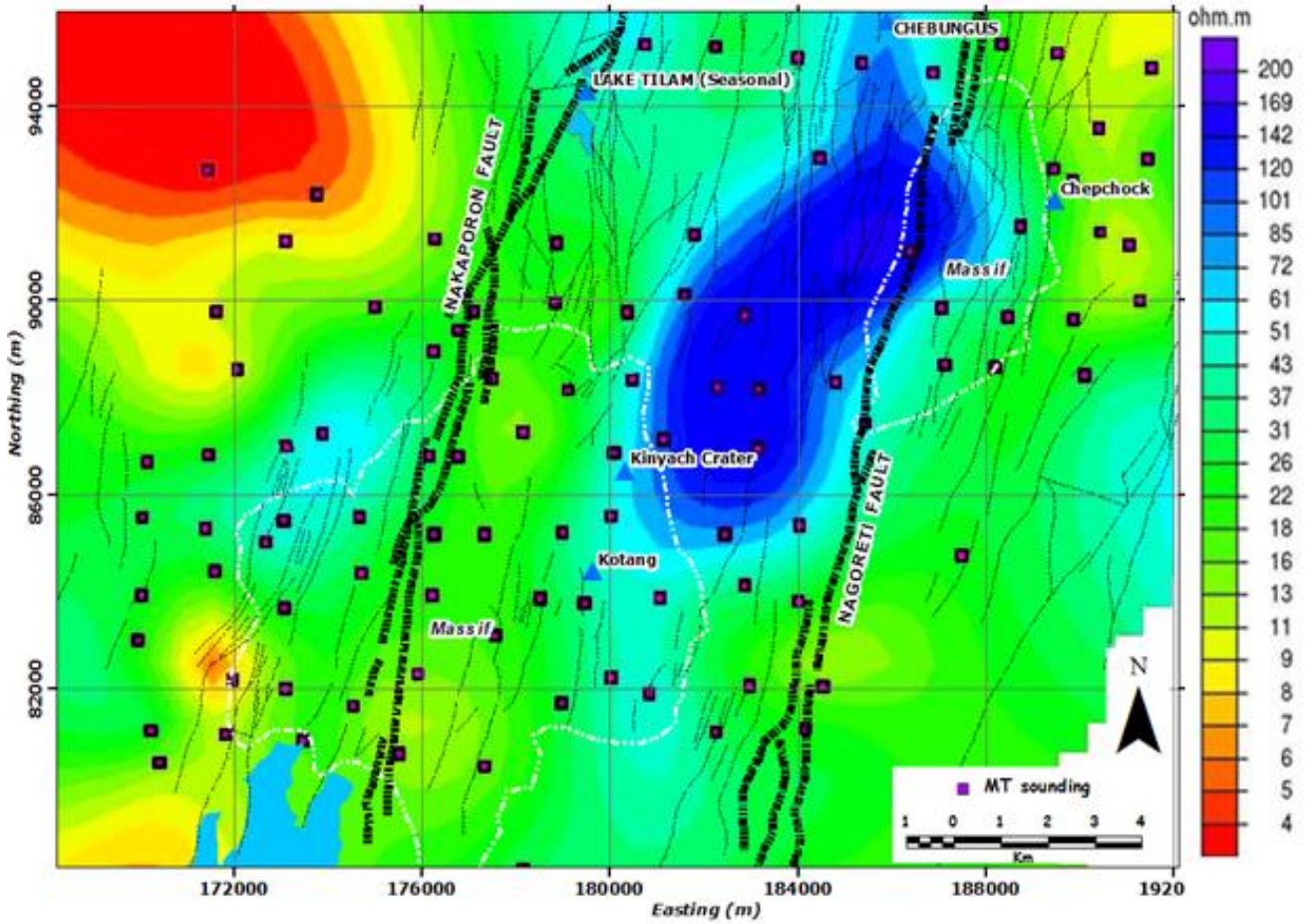

Figure 2-9: Resistivity at 1000m below sea level. Source: Raymond, 2011

d) Resistivity at -3000 mbsl

Examination of the iso-resistivity maps at 3000 mbsl and 4000 mbsl (Figures 2-10 & 2-11) indicate two main trends of resistivity anomalies running parallel to each other in a NNE direction. The first anomaly is of low values of <10 ohm-m connecting the SW sector of the survey through the western half of the Korosi massif. The other anomaly has higher values of between 20 and 100 ohm-m probably a vapour dominated system hosted on the eastern part of Korosi massif running northwards across Kinyach crater towards the western part of Chepchuk massif.

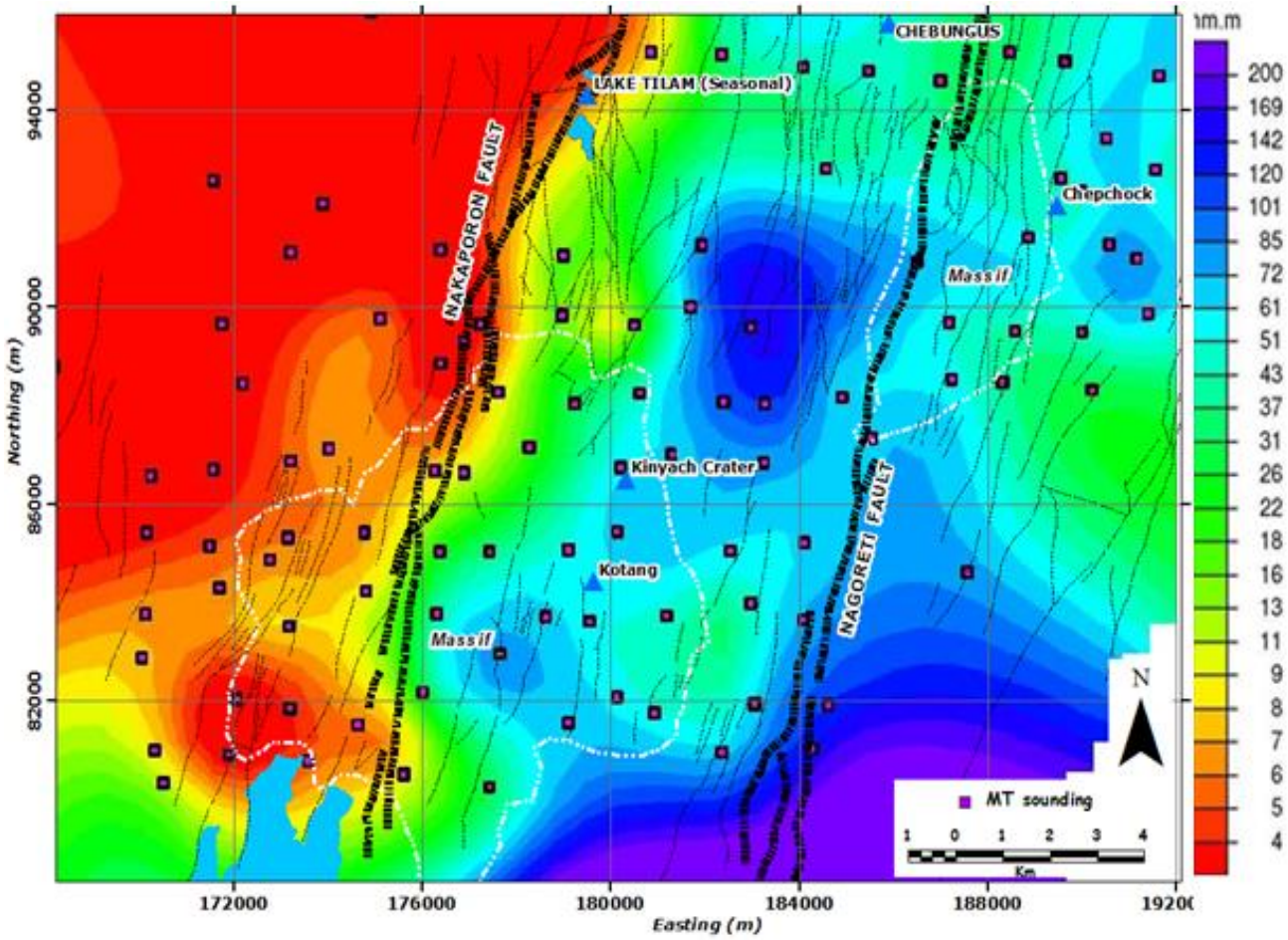

Figure 2-10: Resistivity at 3000m below sea level (mbsl). Source: Deflora, 2011

e) Resistivity at -4000 masl

The low resistivity in the north western part is not well defined at this level because of a few data points but a deep conductor is well defined towards the south western part and is aligned along the major Nakaporon fault which is propably the fluid circulation zone (Figure 2-11).The steam dominated system becomes more pronounced on the central part of the prospect and alighns in the direction of the major structures this is probably a dry steam zone.

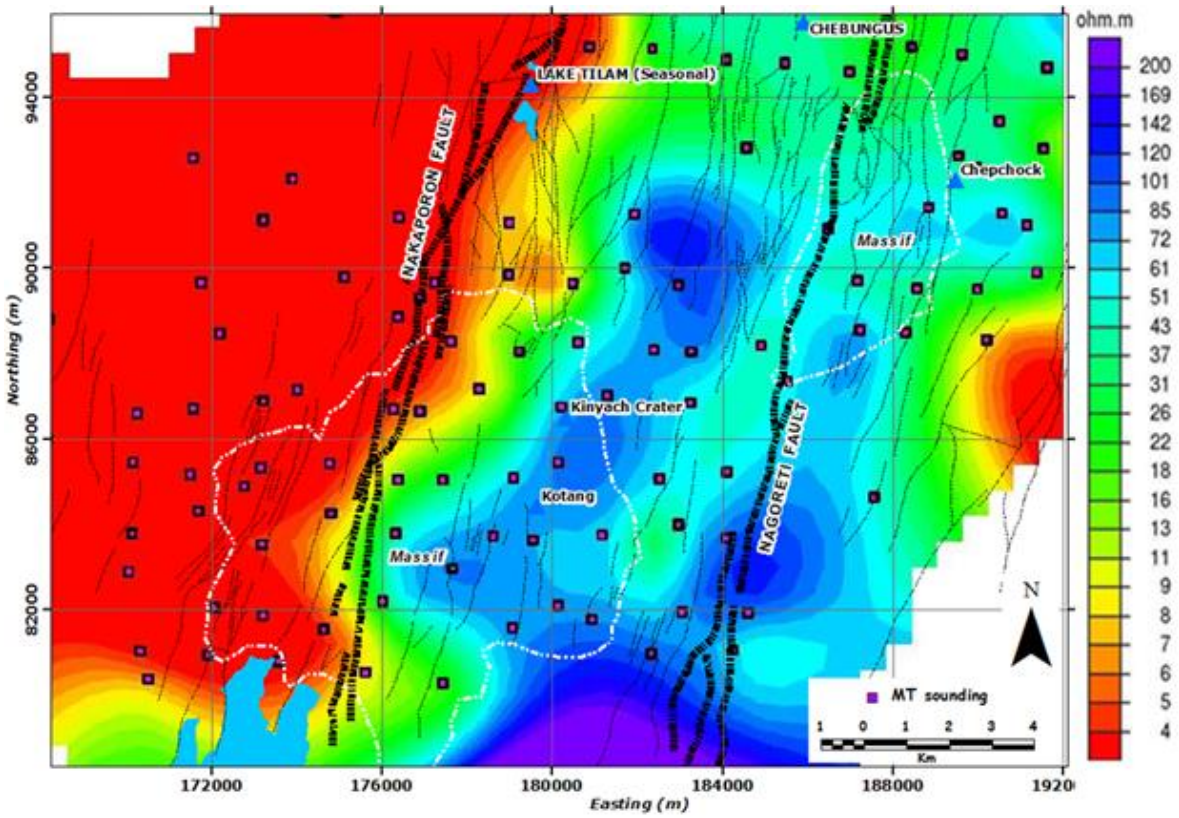

Figure 2-11: Resistivity at 4000m below sea level. Source: Deflora, 2011

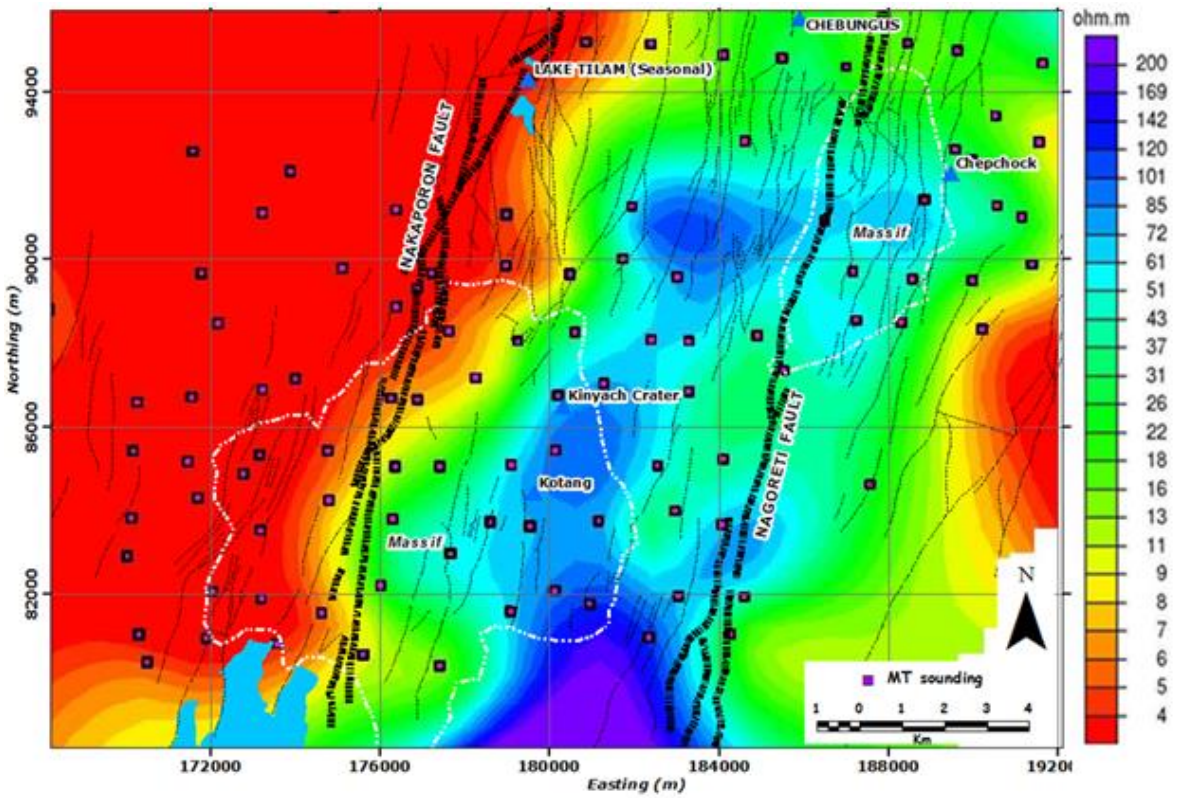

Figure 2-12: Resistivity at 5000m below sea level. Source: Deflora, 2011.

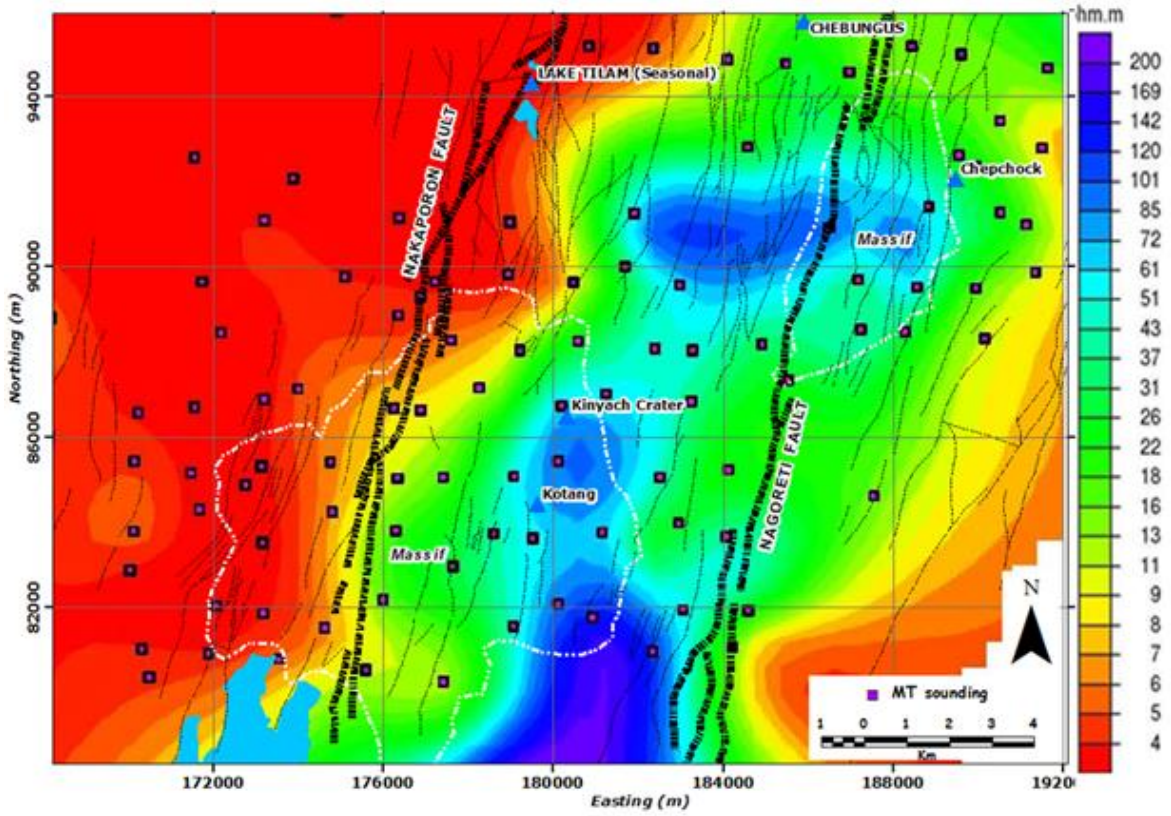

Figure 2-13: Resistivity at 6000m below sea level. Source: Raymond, 2011

f) Resistivity at -5000 masl and -6000masl.

A similar resistivity structure as in the previous plot is seen (Figure 2-10 and 2-11) with the deep conductor becoming more aligned on the western part of the plot and the vapour dominated system alighned along the fault lines on the central parts of the prospect and towards the north eastern part of the plot.

2.5.2 Cross-sections

Cross-section along E-W

The profile cuts through the prospect in a west to east direction (Figure 2-12). A low resistivity layer spreads laterally across the Korosi-Chepchuk prospect which is due to alteration mineralogy near the surface. A highly resistive zone postulated as the vapour system is seen underlying the low temperature alteration zone. The results were based only on 1D inversion of MT data using a WinGlink software. Three exploration wells were sited as shown in Figure 2-13.

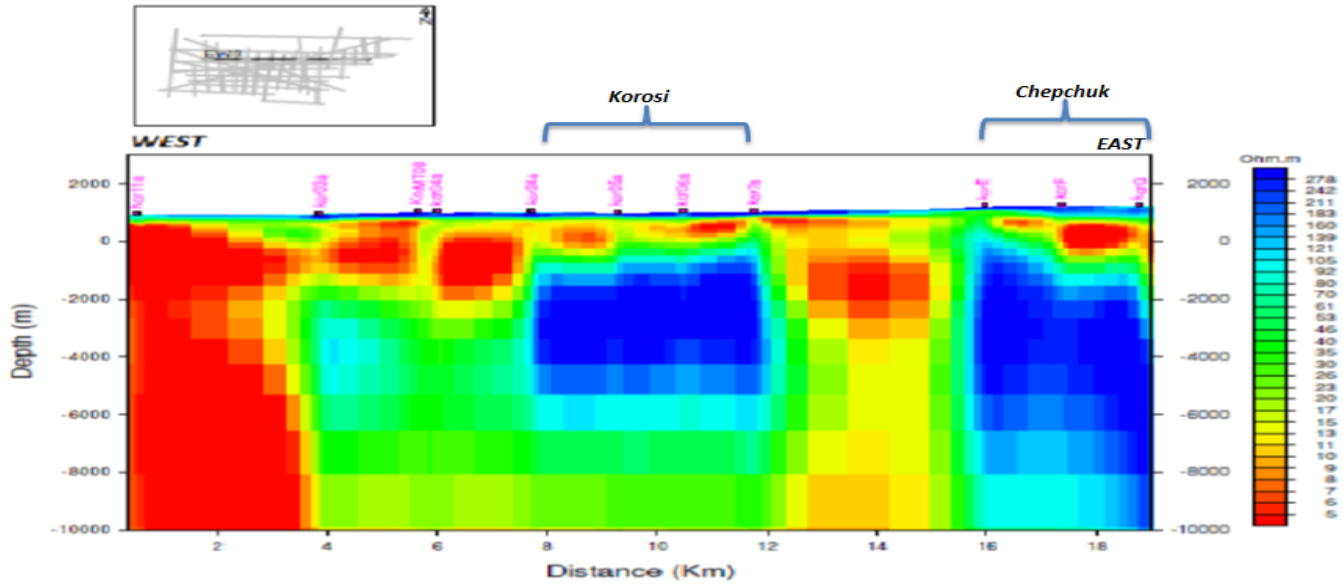

Figure 2-14: 2D Resistivity cross-section along E-W. Source: Raymond, 2011

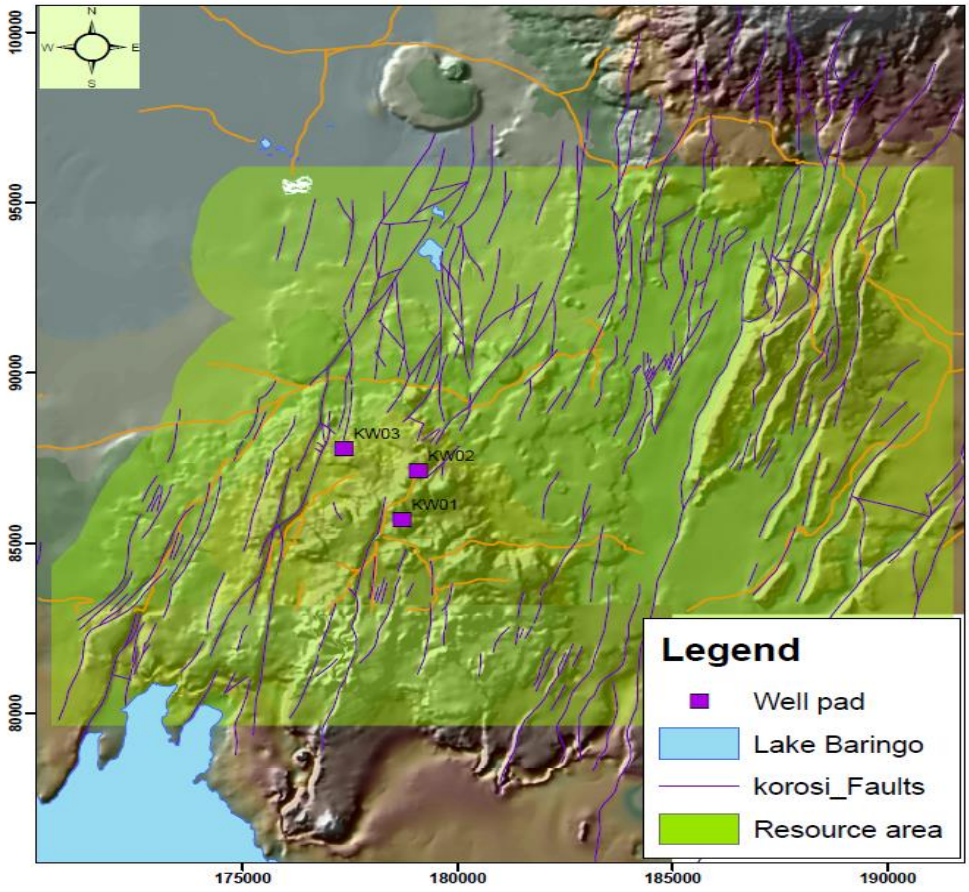

Figure 2-15: Map showing proposed three exploration well sites at Korosi geothermal prospect. Source: Charles, 2014

2.6 Review of methods of data analysis

This part describes available methods of 3D inversion of MT data in brief, reviewing the limitations of model space compared to data space approach to 3D inversion of MT data. The algorithm for inversion shows the basis of the data space method of data inversions and links up the technology advancement to practicality of the inversion process. The reason for choosing the WSINV3DMT for this inversion is discussed in general process of data processing and analysis.

The 3D inversion of MT data has evolved from one dimensional (1D to 2D and then to three dimensional (3D). The Occam's inversion was presented by Constable et al. (1987) for 1D resistivity model using MT data. It was later expanded to 2D MT data resistivity modeling by deGroot-Hedlin and Constable (1990). Occam's inversion is stable, it converges to a desired misfit in relatively few iterations in relation to other available methods. Both these methods are based on the model space approach. The costs of computation associated with formulating and inverting space matrices of a large scale resistivity makes model-space Occam's 3D inversion of MT data unfeasible since all calculations depends on the size of model parameter, M.

These complications may be overcome by use of an approach that is data-space, where matrix dimensions depend on the size of the number of MT dataset N, rather than the number of model parameters M. Generally where N << M for MT data. As argued in Siripunvaraporn and Egbert (2000), the alteration of the inverse problem to the data space can significantly improve the computational efficiency for the 2-D MT problem. WSINV3DMT code is based on the data space approach (Siripunvaraporn et al., 2005). With the makeover to data space the cost of computation (i.e. CPU times and RAM required) are significantly reduced making the 3-D inversion feasible on computers and laptops (Weerachai Siripunvarapron, 2006)

2.7 Review of three-dimension (3D) forward modelling

This type of inversion depend heavily on forward modeling not only for calculating model responses but also sensitivities. An effective and accurate forward modeling code is thus essential (e.g., Mackie et al., 1994; Smith, 1996; Newman and Alumbaugh, 2000; Siripunvaraporn et al., 2002; Avdeev et al., 2002). Maxwell's equations second order with a staggered grid finite difference numerical approximation was done. This approach to 3D forward modeling is flexible and allows large and complicated model structures (depending on computer resources) in an effective way.

There are two forms of the second order Maxwell's equation: in terms of electric fields:

$$\nabla \times \nabla \times \mathbf{E} = i\omega\mu\sigma\mathbf{E}, \quad (3a)$$

or magnetic fields

$$\nabla \times \rho\nabla \times \mathbf{H} = i\omega\mu\mathbf{H}. \quad (3b)$$

Where μ is the air magnetic permeability, ω the angular frequency, σ the conductivity, **E** the electric field, and **H** the magnetic field. Siripunvaraporn et al. (2002) have shown that solutions obtained from equations formulated in terms of the electric fields (3a), with a staggered grid finite difference are less sensitive to grid resolution than those obtained from the magnetic formulation (3b). Therefore, use equation (3a) and not (3b) for modeling electromagnetic data. With a staggered grid finite difference approximation to (3a), discrete system of equations **Ax** = **b** was obtained, where **b** is the boundary electric fields, **x** the unknown interior electric field, and **A** the symmetric coefficient matrix (but **A** is not Hermitian; it consists of complex numbers only on the diagonal). The linear system of equations is therefore solved using quasi-minimum residual (QMR) method, with a pre-conditioner formed by an incomplete LU decomposition of the diagonal sub-matrix of **A** (Siripunvaraporn W. E., 2002). To speed up convergence a divergence correction, similar to Smith (1996), is applied. The iterative solution is terminated once the level of normalized misfit, $\mathbf{r} = ||\mathbf{Ax}-\mathbf{b}||/||\mathbf{b}||$, is below 10^{-7}. After solving for the interior electric fields, the magnetic fields at the surface are then computed and interpolated in the usual way that is by use of first order Maxwell's equations.

The development of 3 dimension inversion codes for MT and progresses in computer capability 3D MT inversion has become attainable. It is thus vital to carry out 3D inversion to determine the true resistivity structure. This was attained using 3D inversion program annotated, WSINV3DMT version 1.1.0 by (Siripunvaraporn W. E., 2005) which pursues to find a model with a response that fits the data. This inversion code use fixed difference forward algorithm and formulates the inversion problem in data-space rather than the more computationally demanding model-space approach. Thus, this scheme to a great extent reduces the computational time and memory required for the inversion making the 3-D inversion of MT data feasible.

2.8 Chapter two summary

All the previous results on Korosi field were established on 1D inversions of MT resistivity data. The inverted resistivity model derived from the 1D inversion cannot be reliable at depth due to complex resistivity structure inherent in volcanic areas. There is no resistivity model derived from higher dimensional inversion of MT data which has been done on Korosi geothermal prospect. 3D inversion of resistivity data refined the resistivity model of the prospect and will help to site wells with more clarity as well as raising the confidence level of the sited wells. 3D inversion is computational demanding but is still remains the best way to recover resistivity structure with higher accuracy in that it is based on a multidimensional approach.

CHAPTER THREE

3.0 RESEARCH METHODOLOGY

3.1 Introduction

The chosen method for this research is 3D inversion of MT resistivity data using data space. The method was arrived at with respect to low Random Access Memory (RAM) and higher chances of convergence into desired results. There is only one code available for 3D inversion using data space approach; WSINV3DMT. Though rigorous the code was chosen for the purpose of this study since the required and available computing facility was based on this method. This chapter seeks to explain the methodical procedure for the 3D inversion of the data set as used in this research.

3.2 Research design

Among several research designs in existence, the research design for this research was a case study research design. This research design befitted all the objectives.

3.3 MT data Quality check

The MT data collected in the years 2006, 2011, and 2015 was checked for quality analysis. The quality check involved frequency analysis, smoothness, phase and presence of the static shift in the data. Frequency analysis is a vital undertaking was used to determine the skin depth and possibility of static shift correction using TEM inter alia. The smoothness check involved subjecting the individual soundings into a spline smoothing algorithm and consequent fixing of the outliers. Phase is an important parameter to view as it exhibits if proper or improper layout was done in the field. In case the layout was not well then corrective measures were done to reverse the same using the SSMT200, if not possible then the data shall was not used in this research. Only high quality (less noisy) data were selected for use in this research. Data quality check disregarded several soundings that reduced the model size. The quality of MT data used is shown at the appendixes.

Figure 3-1 Indicate the type of raw data from the machine annotated with suffix "(o)" and semi processed data from the WinGlink annotated with suffix "(e)". Freq. in the figure 3-1 means frequency, Rho XY (o), Rho XY (e), Phi XY (o), Phi XY (e) means apparent resistivity and phase respectively both original (o) and smoothed (e) in the North-South (XY) and East-West(YX) directions respectively.

Station: KORMT123

Freq.	Rho XY (o)	Rho XY (e)	Phi XY (o)	Phi XY (e)	Rho YX (o)	Rho YX (e)	Phi YX (o)	Phi YX (e)
320.0000	7.6296E+01	1.2301E+02	7.3005E+01	7.3005E+01	1.5376E+02	1.0714E+02	-1.1500E+02	-1.1500E+02
265.0000	7.2048E+01	1.1616E+02	7.3935E+01	7.3935E+01	1.4660E+02	9.9296E+01	-1.1423E+02	-1.1423E+02
229.0000	6.5983E+01	1.0639E+02	7.3656E+01	7.3656E+01	1.3785E+02	9.3372E+01	-1.1462E+02	-1.1462E+02
194.0000	5.8733E+01	9.8079E+01	7.4216E+01	7.4216E+01	1.2649E+02	8.5673E+01	-1.1413E+02	-1.1413E+02
159.0000	5.3664E+01	8.7982E+01	7.4565E+01	7.4565E+01	1.1779E+02	7.9784E+01	-1.1399E+02	-1.1399E+02
132.0000	4.8090E+01	7.8845E+01	7.3653E+01	7.3653E+01	1.0786E+02	7.3058E+01	-1.1505E+02	-1.1505E+02
115.0000	4.6215E+01	7.2305E+01	7.2693E+01	7.2693E+01	1.0225E+02	6.9260E+01	-1.1608E+02	-1.1608E+02
97.0000	4.1397E+01	6.3691E+01	7.2103E+01	7.2103E+01	9.4026E+01	6.3687E+01	-1.1695E+02	-1.1695E+02
79.0000	3.6289E+01	5.5833E+01	7.1778E+01	7.1778E+01	8.7340E+01	5.7887E+01	-1.1735E+02	-1.1735E+02
66.0000	3.0463E+01	4.9115E+01	7.2111E+01	7.2111E+01	7.8596E+01	5.3235E+01	-1.1721E+02	-1.1721E+02
57.0000	2.7854E+01	4.4909E+01	7.1470E+01	7.1470E+01	7.4830E+01	4.9972E+01	-1.1731E+02	-1.1731E+02
49.0000	2.2193E+01	3.9856E+01	7.1019E+01	7.1019E+01	6.3721E+01	4.6006E+01	-1.1768E+02	-1.1768E+02
40.0000	2.1576E+01	3.5368E+01	6.9829E+01	6.9829E+01	6.2219E+01	4.2143E+01	-1.1915E+02	-1.1915E+02
33.0000	1.9558E+01	3.1534E+01	6.8671E+01	6.8671E+01	5.8100E+01	3.9353E+01	-1.2032E+02	-1.2032E+02
27.5000	1.7762E+01	2.8638E+01	6.7792E+01	6.7792E+01	5.4792E+01	3.7241E+01	-1.2111E+02	-1.2111E+02
22.5000	1.5957E+01	2.5727E+01	6.6853E+01	6.6000E+01	5.0170E+01	3.5244E+01	-1.2253E+02	-1.2253E+02
18.8000	1.5480E+01	2.4044E+01	6.6528E+01	6.4800E+01	5.0389E+01	3.3661E+01	-1.2379E+02	-1.2379E+02
16.2000	1.4161E+01	2.2831E+01	6.6114E+01	6.4385E+01	4.6725E+01	3.2595E+01	-1.2474E+02	-1.2474E+02
13.7000	1.3244E+01	2.0948E+01	6.5098E+01	6.1845E+01	4.7606E+01	3.1802E+01	-1.2583E+02	-1.2583E+02

Figure 3-1: A section of pre-processed data ready for static shift inversion.

3.4 Procedure of data processing and design of input files to WSINV3DMT code.

MT sounding data collected using Phoenix MTU-5A, 5 channel data logger from Korosi geothermal area was subjected to robust processing using SSMT2000 to convert the data from time domain to frequency domain. The data was further converted into *.EDI by use of MT editor. Apparent resistivity and phase values were achieved using WinGlink software (Figure 3-2). Smoothing was done in both the MT editor and WinGlink software and checked by splsm_mt00.jav, a spline smoothing code developed by Honda (West JEC) in 2014. On WinGlink all data were rotated to user defined angle so as to allow multidirectional orientation of structures. WinGlink software was also used to perform preliminary static shift correction using transient electromagnetic (TEM) data (Figure 3-3). Performing final static shift correction, plots of apparent resistivity maps of 0.1 Hz, 1Hz, 10Hz, 100Hz were obtained using Golden Software Suffer version 11, a plot that is near surface (e.g at 100Hz) is most appropriate for use

to do final static shift correction. This is because the static shift is due to near surface inhomogeinities. The final static shift (Figure 3-4) correction was calculated as a ratio of Log base 10 of smoothed apparent resistivity to Log base 10 of original apparent resistivity at a frequency reflecting resistivity structure near the surface.

An *.awk code (ws3dinpCrr04-GDC) was used to recalculate impedance elements using the corrected apparent resistivity and phase values as input file. Impedance elements were geo-referenced by model coordinates of the individual stations to form the data input file for WSINV3DMT code. From the wide frequency spectrum a representative 16 periods were chosen for inversion. At each period impedance elements Zxy, Zyx both real and imaginary (Figure 3-5) were selected for inversion. An initial model file (Figure 3-6) was made taking into account the distribution of the stations, grid configuration and initial resistivity model boundary condition were determined by the model mesh used. Design of other parameters that form input files was performed and a 3D inversion was done using data space approach code WSINV3DMT developed by Siripunvaraporn. A high end 64 GB RAM, 1TB ROM, 16 Core computer with hyper threading capability was used to perform the inversion. The inversion took 36 hours for the first run and 34 hours for the second confirmation run. The code employs an iterative mathematical model to fit the observed data to the calculated model. The ideal RMS is usually one. This cannot be achieved usually but the closer the resulting RMS to this ideal (RMS =1) the closer results to the true resistivity. A minimum RMS of 1.3171 (Figure 3-7) was obtained at iteration 12 above which the RMS started to increase. Model results of iteration 12 were taken as the best solution and imaged to obtain the 3D resistivity model of Korosi geothermal prospect using Surfer and Voxler softwares.

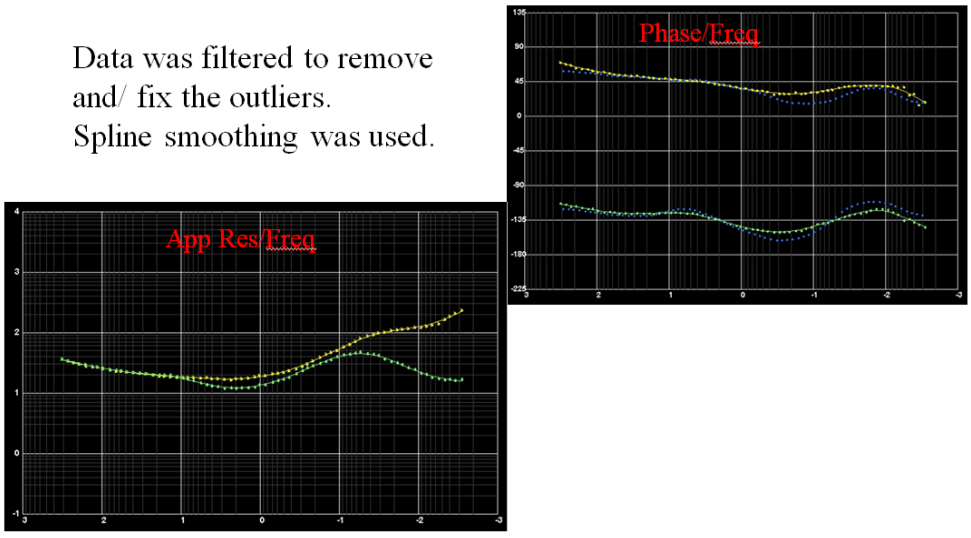

Figure 3-2: Screenshot of data analysis showing plotted Phase/Frequency and Apparent Resistivity/Frequency curves. Source: Arthur M. M., 2016

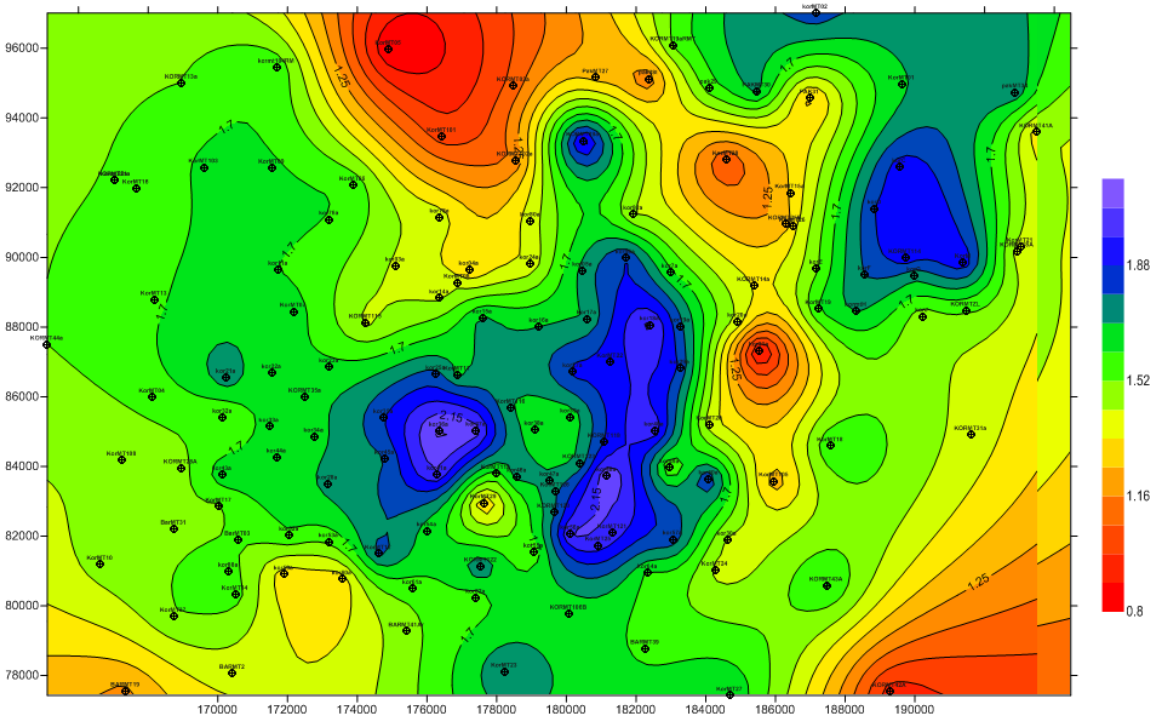

Figure 3-3: Preliminary static shift with TEM data. *(The scale in this figure is in log scale with 0.8, 1.16,1.52, 1.88 representing 6.309, 14.45, 33.11, 75.85 ohm-m).* Source: Arthur M. M., 2016

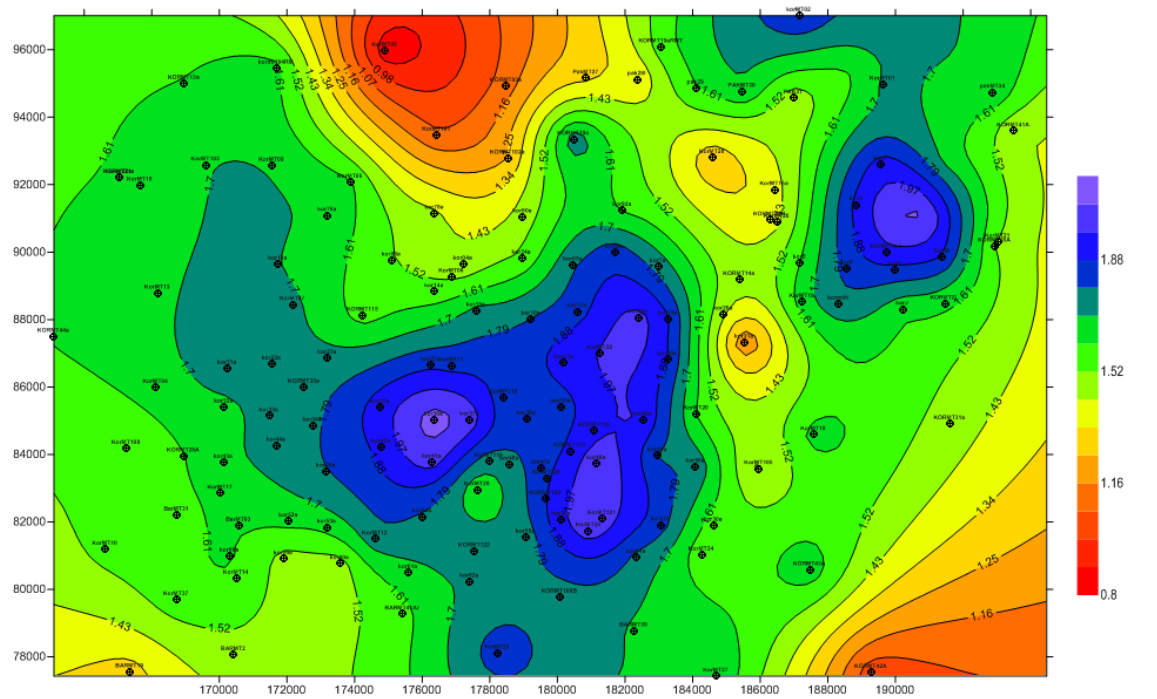

Figure 3-4: Final static shift correction. *(The scale in this figure is in log scale with 0.8, 1.16,1.52, 1.88 representing 6.309, 14.45, 33.11, 75.85 ohm-m)*. Source: Arthur M. M., 2016

Only pairs of MT and TEM stations were chosen for this 3D inversion. TEM stations that were 300m or less from MT station were also taken into account for this MT 3D inversion.

Zxy Zyx

```
+4.1952E-002 -1.7886E-001 -6.0574E-002 +1.7692E-001
+1.2618E-001 -1.7477E-001 -1.2323E-001 +1.7405E-001
+4.8896E-002 -1.0739E-001 -4.7547E-002 +1.0930E-001
+6.7776E-002 -1.6775E-001 -5.9384E-002 +1.7246E-001
+7.7749E-002 -1.8496E-001 -9.2947E-002 +1.7666E-001
+9.3405E-002 -2.3591E-001 -1.1090E-001 +2.2389E-001
+2.3611E-002 -6.7801E-002 -4.3611E-002 +5.6896E-002
+4.9746E-002 -1.7817E-001 -9.7351E-002 +1.5598E-001
+7.1584E-002 -1.9095E-001 -6.6686E-002 +1.9032E-001
+5.7938E-002 -1.4015E-001 -4.4627E-002 +1.4470E-001
+1.1076E-001 -1.6255E-001 -1.1179E-001 +1.6073E-001
+4.4871E-002 -1.5857E-001 -5.3944E-002 +1.5490E-001
+1.0974E-001 -1.9765E-001 -1.1388E-001 +1.9621E-001
+1.2402E-001 -2.1327E-001 -1.1745E-001 +2.1695E-001
+5.1567E-002 -1.8482E-001 -5.2288E-002 +1.8528E-001
+7.0687E-002 -1.6374E-001 -7.3020E-002 +1.6248E-001
```

R jx R jx

Figure 3-5: A section of impendance elements (Zxy and Zyx) at a particular period with both real (R) and Imaginaly elements (jx). Source: Arthur M. M., 2016

```
58 77  28   1
  34000.00  17000.00   8500.00   4500.00   2500.00   1500.00
    950.00    650.00    500.00    500.00    500.00    500.00
    500.00    500.00    500.00    500.00    500.00    500.00
    500.00    500.00    500.00    500.00    500.00    500.00
    500.00    500.00    500.00    500.00    500.00    500.00
    500.00    500.00    500.00    500.00    500.00    500.00
    500.00    500.00    500.00    500.00    500.00    500.00
    500.00    500.00    500.00    500.00    500.00    500.00
    500.00    500.00    650.00    950.00   1500.00   2500.00
   4500.00   8500.00  17000.00  34000.00
  34000.00  17000.00   8500.00   4500.00   2500.00   1500.00
    950.00    650.00    500.00    500.00    500.00    500.00
    500.00    500.00    500.00    500.00    500.00    500.00
    500.00    500.00    500.00    500.00    500.00    500.00
    500.00    500.00    500.00    500.00    500.00    500.00
    500.00    500.00    500.00    500.00    500.00    500.00
    500.00    500.00    500.00    500.00    500.00    500.00
    500.00    500.00    500.00    500.00    500.00    500.00
    500.00    500.00    500.00    500.00    500.00    500.00
    500.00    500.00    500.00    500.00    500.00    500.00
    500.00    500.00    500.00    500.00    500.00    500.00
    500.00    500.00    500.0     650.00    950.00   1500.00
   2500.00   4500.00   8500.00  17000.00  34000.00
     25.00     25.00     31.00     39.00     49.00     61.00
     76.00     95.00    119.00    149.00    186.00    233.00
    291.00    364.00    455.00    568.00    711.00   1066.00
   1599.00   2398.00   3597.00   5396.00   8094.00  12140.00
  18210.00  27316.00  40973.00  61460.00
   15
   1   28
 1 1 1 1 1 1 1 1 1 1 1 1 1 1 1 1 1 1 1 1 1 1 1 1 1 1 1 1 1 1 1 1 1 1 1 1 1 1 1 1 1 1 1 1 1 1 1 1 1 1
```

N-S: 500m model cells for internal grid and 8 cells on each side for boundary conditions where change of electric field is assumed to be zero.

E-W: 500m cells for internal grid and 8 cells on each side for bounday conditions for electric field

Z: 28 layer in the vertical direction starting from 25m below the surface

15: Averange resistivity value for the whole field

1 28: 28 layer from the surface

Innitial resistivityof 10 ohm-m to start iteration

Figure 3-6: Initial model file taking into account the boundary conditions for the electric field.. Source: Arthur M. M., 2016

From figure 3-6: The values 58, 77, 28, 1 denote number of cells in the North-South direction, East – West direction, Number of layers and number of resistivity values respectively. It presents the initial model design which spans 34kM on both North South and East West and 61.4kM for the depth on internal model design. The boundary conditions are taken from when the Electric field is equal to zero (E = 0).

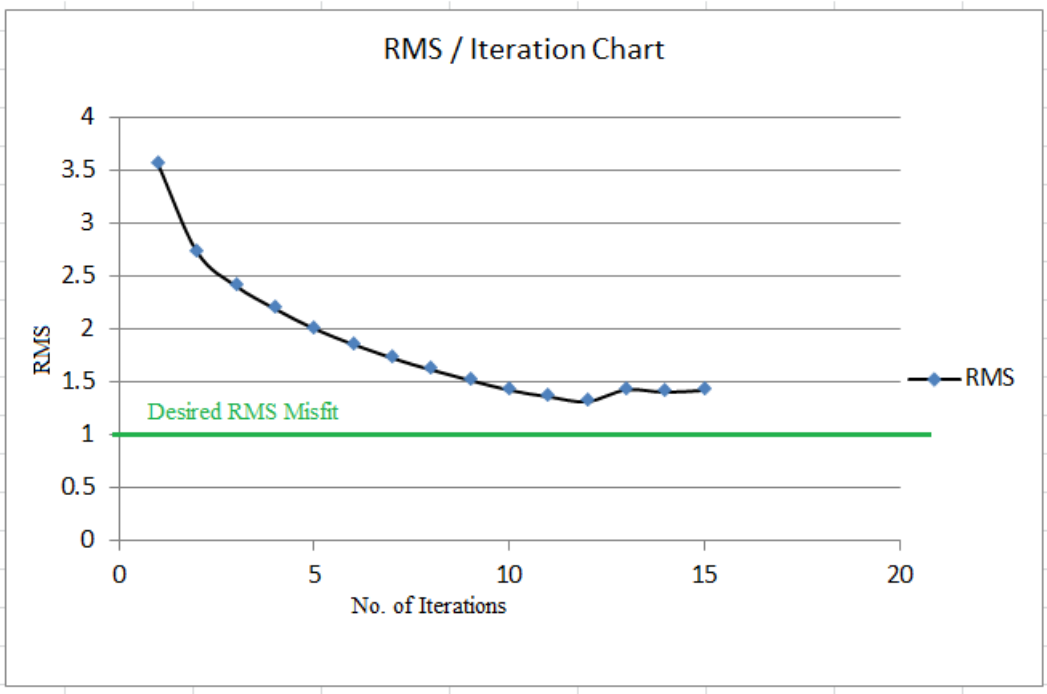

Figure 3-7: A plot of Root Mean Square (RMS) verses Iteration showing RMS trend during inversion. A maximum iteration of 15 was set for each run. Source: Arthur M. M., 2016

3.5 Chapter three summary

The WSINV3DMT inversion code is based on the data space approach (Siripunvaraporn et al., 2005). With the transformation to data space the computational costs (i.e. CPU times and RAM required) are significantly reduced making the 3D inversion practical for PCs and workstations. (Weerachai Siripunvaraporn et al. 2006). The inversion converges with relatively smaller number iteration as opposed to a model space codes. Design of the input files is rigorous and requires much time, commitment and accuracy in order to obtain a reliable inverted resistivity model.

CHAPTER FOUR

4.0 RESULTS AND DISCUSSION

4.1 Introduction

This chapter presents 3D inversion findings derived from smoothed 10 ohm-m consistent half-space initial model. Normally the 3D code assumes a level surface, but as stated previously the MT data were corrected for static shift before inversion and this correction significantly eliminates topographic effects in the data. The resistivity models resulting from the inversion were elevation corrected, and results are presented in ISO surfaces and maps, section and volumetric resistivity models.

4.2 Data Coverage

147 MT sounding were prepared for three dimensional inversions. Some south east parts were not very covered due to rough terrain which barred accessibility. The sounding distribution (Figure 4-1) was fairly representative of the area with density of less than 1km spacing on average except SE part of the prospect. A face render resistivity block of the prospect is plotted (Figure 4-1). The quality of the MT data used for this inversion is shown at the appendixes.

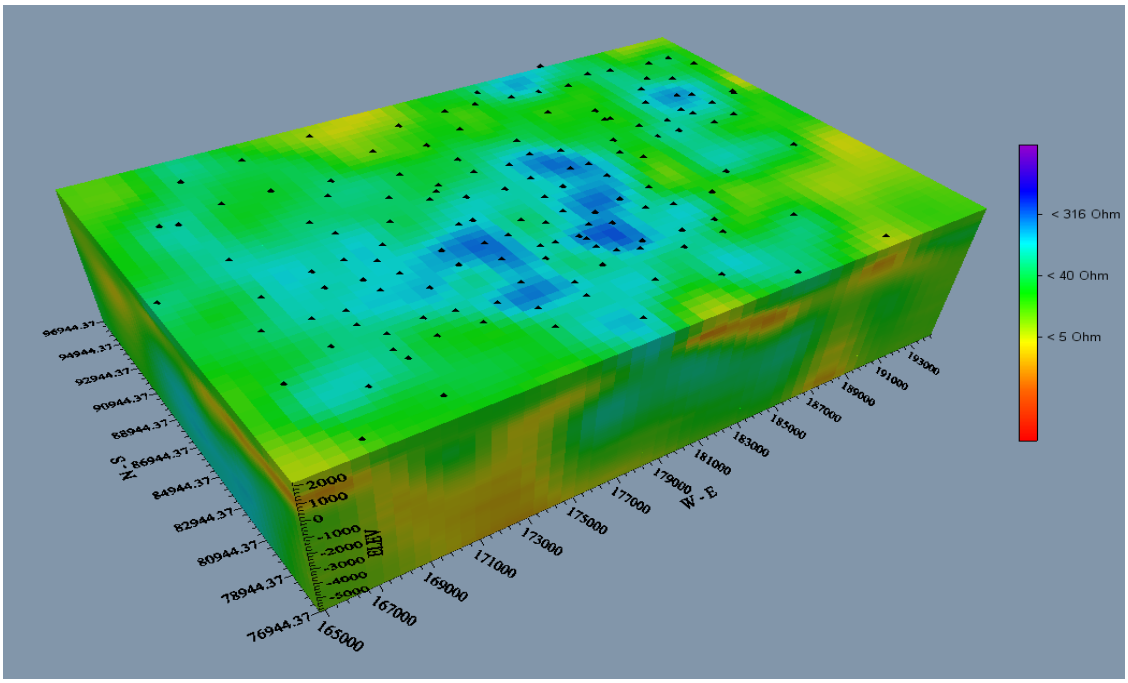

Figure 4-1: A block resistivity model of Korosi – Chepchuk is shown with MT/TEM soundings overlaid *(The black triangles indicate density of MT/TEM soundings).*

4.3 Three dimensional inversion results

The results of the inversion were achieved after iteration number 12. Root mean square (RMS) is one of the measure of the best results. The lowest RMS is not always the desired result, analysis of the results is key to a good and realistic interpretation. The closer the results to unity the better closer the results are to the desired results.

The objective of this study was to recover the general resistivity structure of the Korosi Geothermal Prospect as exhibited by figure 4-2.

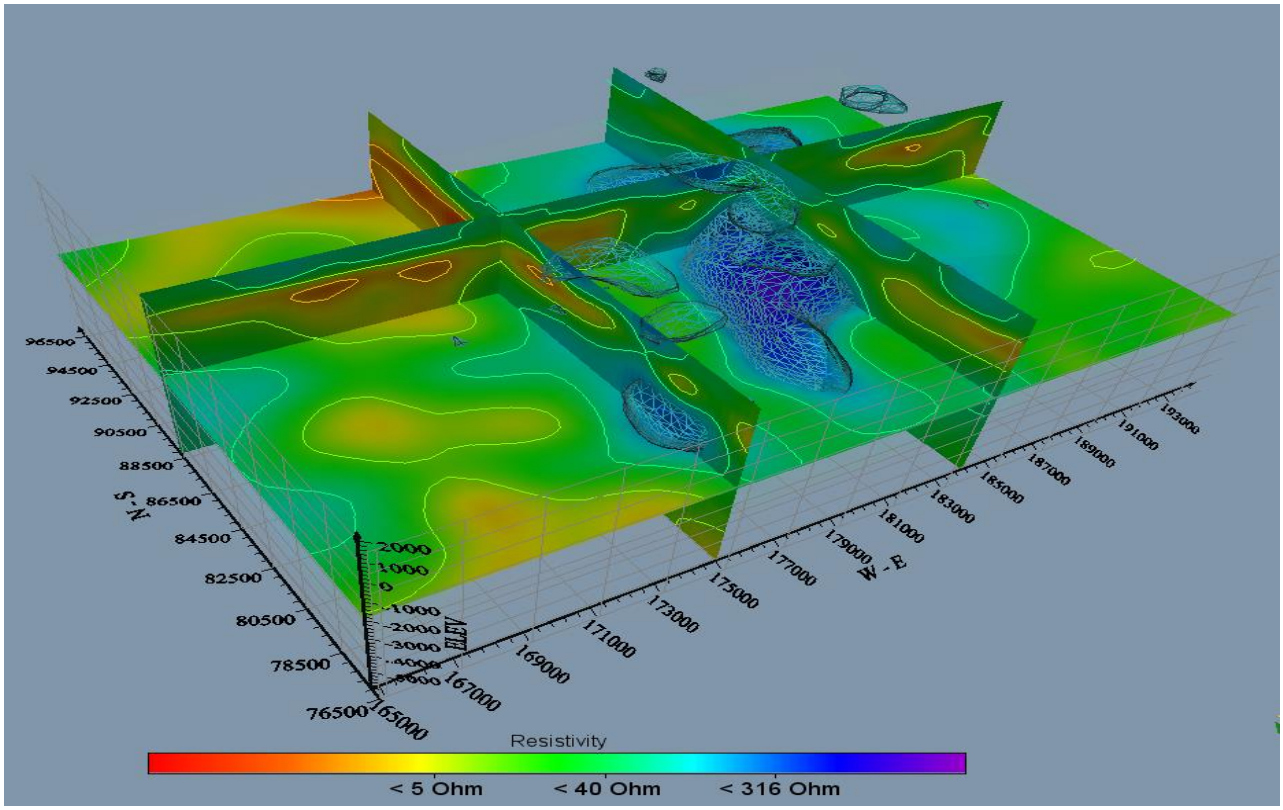

Figure 4-2: W-E and N-S and ISO resistivity sections of Korosi geothermal prospect

The first N-S cross- section from left cut through the inferred smaller reservoir and the second N-S cross section from left cut through the second inferred larger reservoir (Figure 4-2).

Resistivity cross sections derived from the inversion results at iteration 12 are observed. Near the surface, < 1000m from surface, a low resistivity is evident inferring possible clay cap. On the surface a high resistivity overburden is seen probably as a result of volcanic lavas as evident on the surface. Uplifted high resistivity zone at depth could infer hydrothermally altered zone formed under high temperature condition, necessitated by remarkably low resistivity zone distributed above the uplifted high resistivity zone. The resistivity discontinuities often reflect

fractured zones along fault lines as shown in figure 4-2. An extensive low resistivity is evident western side of the prospect; this low resistivity could be as a result of sedimentation.

One of the specific objectives for this study was to define the depth of the inferred geothermal reservoir which is exhibited by careful analysis of figure 4-3. The high resistivity overburden on the upper part of the recovered model (figure 4-3) slightly between 1500 and 2000 masl could be the unaltered mineralogy of pumice and other ashy minerals as in figure1-4. The low resistivity layer immediately below this level is the clay capping due to low temperature minerals.

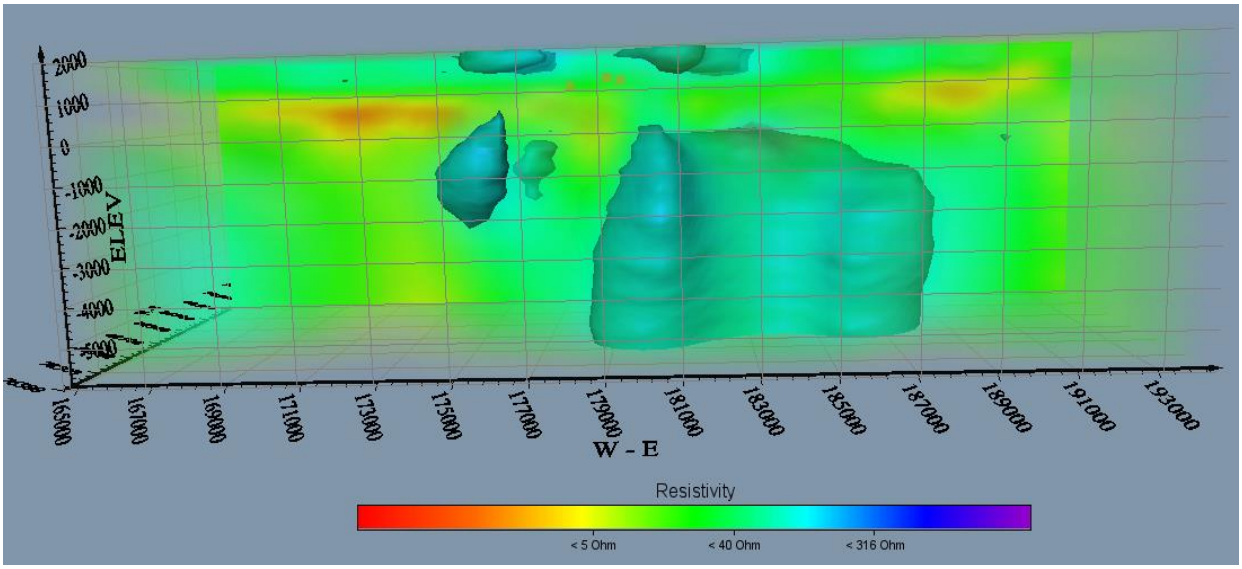

Figure 4-3: Line of constant resistivity of about 125 Ohm-m surface inferring possible reservoir locations in the prospect.

Transparent volumetric block resistivity distribution is overlaid onto a W-E cross section to demonstrate clay capping level and inferred reservoirs (Figure 4-3). A line of constant resistivity of 125 Ohm-m is shown mapping out low resistivity area. This isolates the near surface anomalies as a result of resistive overburden giving a resistivity of several tens of ohm-m to some few hundreds of ohm-m. This overburden is composed of resistive rocks such as muguerite lava, trachyte lava and basalt (Simiyu, 2010). The lower resistivity immediately below this overburden could infer lower temperature mineralogy of clay minerals. This zone appearing at about 1000 masl could infer clay capping of the geothermal reservoir. An up domed high resistivity zone below zones this capping could infer a high temperature where alteration processes may increase the resistivity of some rocks by changing the resultant secondary minerals such as smectite to illite or chlorite which can be interpreted as a geothermal reservoir. The above thus achieves the first specific objective.

As the specific objective sought to define the extent of the geothermal reservoir, two reservoirs are inferred both which are slightly above sea level with the left smaller reservoir superficial relative to the left larger reservoir. The general orientation of the regional structure is evident on the topographic map as NNE-SSW. These form conduits through which hotter fluids transmission is possible to the fumaroles. All the fumaroles KF1-KF4 and CF1-CF3 indicated by red squares are of about 70°C and above indicating some permeability as evident by micro faults (figure 4-
5).

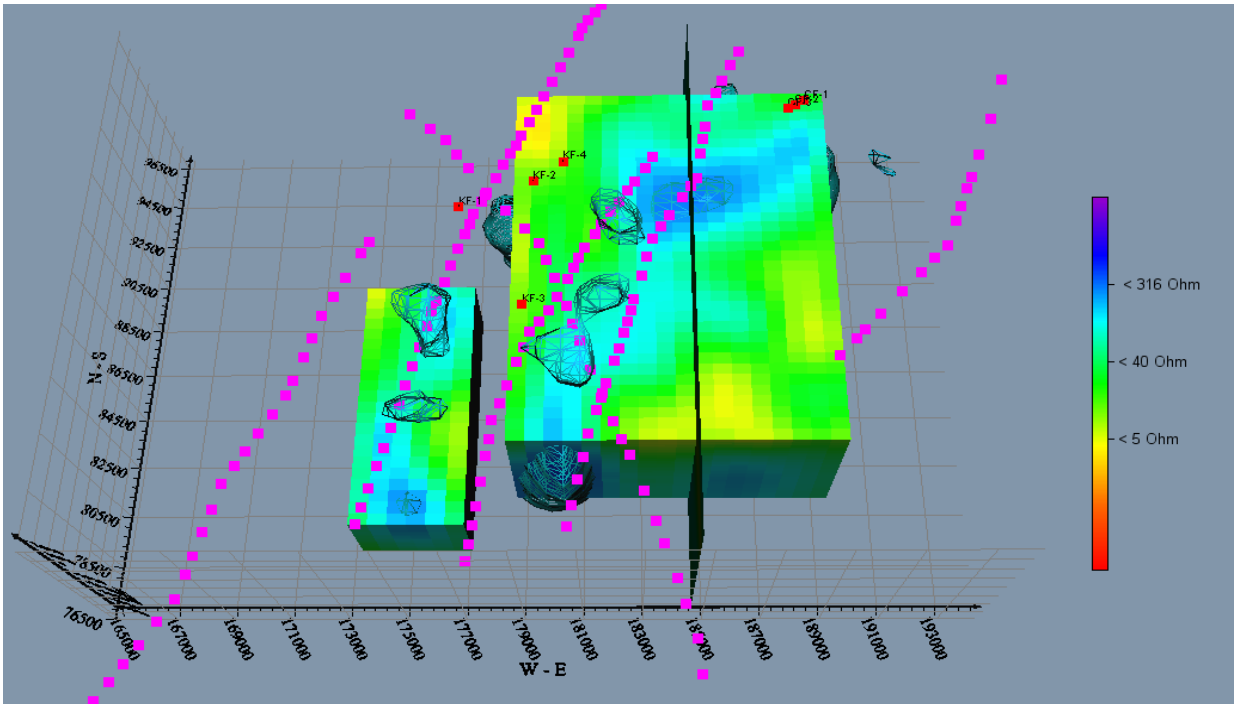

Figure 4-4: Relationship of the inferred reservoir and the regional structures and surface manifestations (fumaroles).

Figure 4-4 and 4-5 sought to fulfill the requirements of the specific objective that relates the surface manifestations to the recovered 3D resistivity model. Red squares are fumaroles. The light purple square lines are regional structures evident on the surface. The two blocks are the two infered geothermal reservoirs. At the intersetions of the geological structures there are fumamaroles. For example KF1 on figure 4-4 is at the intersection of two geological structures which could be the conduits through which high temperature fluids find way to the surface. There are more fumaroles on the left infered geothermal reservoirs than there are in right larger reservoir which would indicate that this region is more fructured and thus transmission of geothermal fluids to the surface.

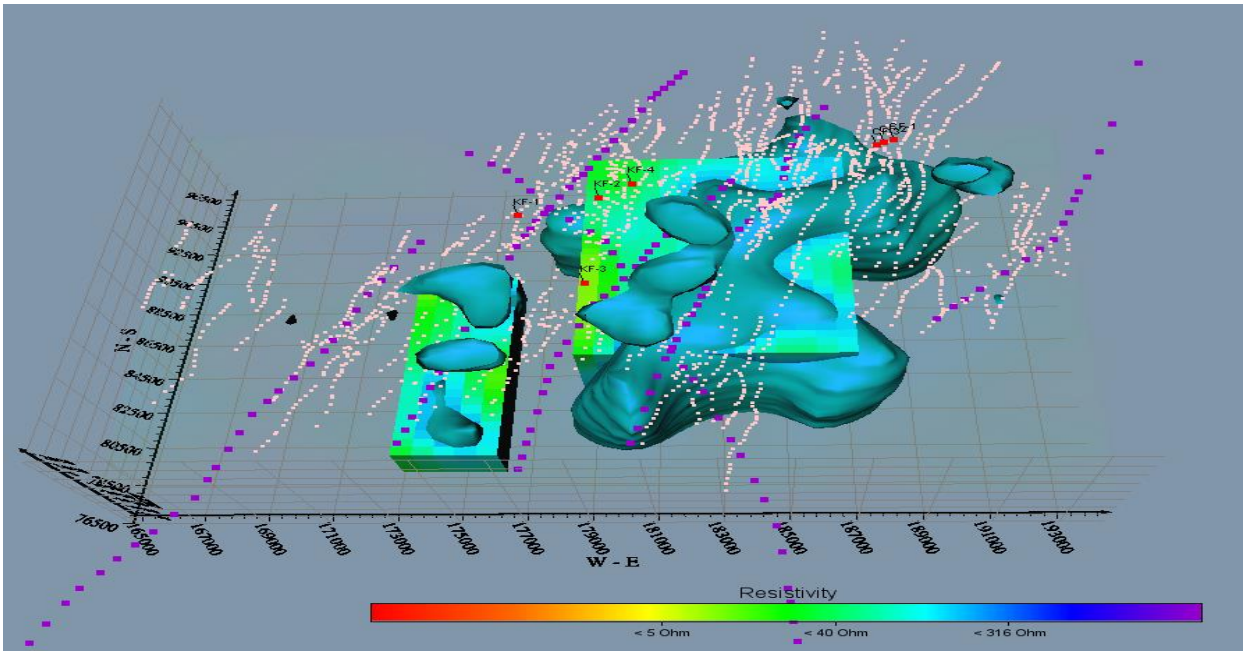

Figure 4-5: Overlay of regional structures onto the 3D resistivity model recovered from 3D inversion analysis. (Regional structures are shown by purples squares and micro faults are indicated by pink dotted line)

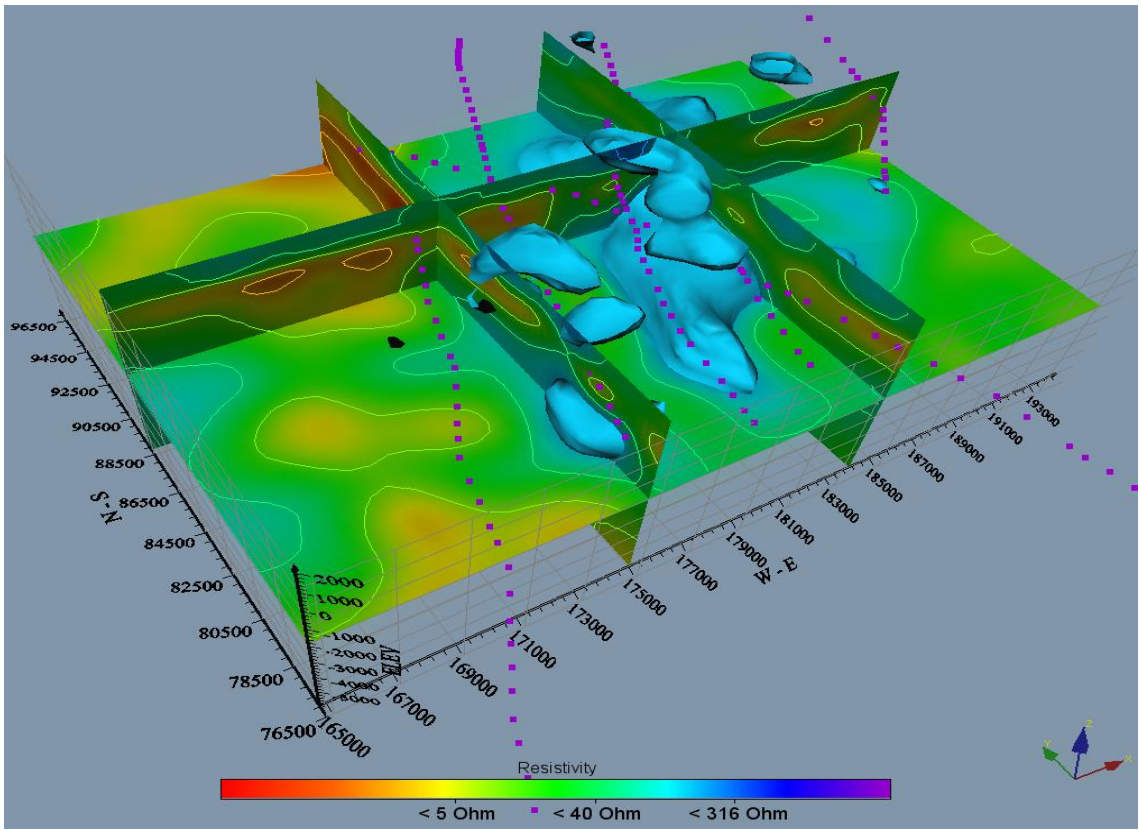

Figure 4-6: Two N-S, one W-E sections speculating the order of resistivity from surface to deeper portion. An ISO resistivity across the reservoirs is shown (Figure 4 6) at approximately

1000mbsl. (The solid bodies (in cyan color) indicate the location of the infered reservoir. A line of constant resistivity of 125 Ohm-m is shown in figure 4-6 indicating boundaries of possible high temperature zones. Major structures (purple squares) deduced from topographic map are also overlaid to indicate fault lines evident on the surface. The W-E cross section and N-S cross sections map out the clay cap. The up domed relatively high resistivity could infer geothermal reservoirs.

3D inversion of MT for the off-diagonal impedance tensor for 147 MT sites and 16 periods discovered the key parts of the subsurface resistivity structures at the Korosi Geothermal Prospect. The resistivity models discovered a representative resistivity structure for a high-temperature geothermal field as found in other areas i.e. a low-resistivity cap underlain by a resistive core which apparently is correlated to the geothermal reservoir (Flóvenz et al., 1985; Eysteinsson et al., 1994; Árnason et al., 2000).

Low-resistivity anomaly detected at superficial depth predominantly around the massive and to the North of the massive is caused by low temperature alteration minerals. The underlying high resistivity is associated with the change in alteration minerals to higher temperature mineralogy within the massive spreading to North of the massive. 6 km deep, a conductive segment are predominant; this deeper high-conductivity area are associated with occurrence of partial melt which could be interpreted as the source of heat for the geothermal system in this field. Nevertheless, it ought to be noted that resolution of MT data at long period perhaps are not trusted due to data levels being close to noise floor, this therefore emphasizes the importance of acquisition of high quality data mostly at long periods. Results from models shown above indicate that resistivity structure up to a depth of 6 km is stable below which models may not be trusted

CHAPTER FIVE

5.0 CONCLUSION AND RECOMMENDATIONS

5.1 Review of the research objectives

The main objective of this research was to interpret the general resistivity structure, analyse the extent of geothermal potential using 3 dimensional inversions of Magnetotelluric (MT) resistivity data derived from Korosi Geothermal Prospect to assist in future prospecting for geothermal resources. Figure 4-2 shows the recovered 3D resistivity model which achieves partly the main objective of this study.

The specific objective of achieving 3D resistivity model for the prospect was achieved by carefully analysing and interpreting figures 4-2 through 4-6 where a typical geothermal systemwas exhibited. Definition of the depth of the geothermal reservoir was achieved by figure 4-3. The depth of the inferred reservoir was at sea level. Comparison and relating 3D resistivity model with surface geothermal manifestations and geological structures was another specific objective which was achieved by figure 4-5 and 4-6 which sought to relate the fumaroles, geological structures and the 3D resistivity model. The key finding in for this specific objective was that there was a close correlation of the three such that intersection of the surface geological structures forms the conduits where passage of the geothermal fluids is to the surface. Sharp contrast of high and low resistivity indicated resistivity anomalies which closely relate to the regional geological structures (figure 4-6).

5.1 Conclusion

This research has proved practicality of 3D inversion of MT with real field data. 147 MT and TEM data acquired from Korosi prospect was used for this research. The general resistivity structure indicates a geothermal potential in Korosi prospect. The lineaments (regional structures) observed from the surface correlate to the resistivity discontinuities observed from the 3D inversion model. MT data inversion results indicate that there exists a typical geothermal system in Korosi – Chepchuk geothermal prospect. The results infer possibility of existence of two geothermal reservoirs within the prospect (Figure 4-4). A low resistivity structure exists between the inferred reservoirs thus dividing it into two. The left smaller reservoir is superficial relative to the larger right reservoir (Figure 4-3). The reservoir depth is estimated to be about 0 Masl. A thin high resistivity overburden (above 200 Ohm.m) of about 500m is seen from the 3D resistivity model, A resistivity of below 10 Ohm.m appears below the resistivity overburden and was deduced to be a

clay mineral of about 800m is seen from the west of the prospect which is probably as a result of sedimentation. An up domed high resistivity at approximately the middle of the prospect indicates a possible reservoir for geothermal development. There could be a steam cap at around 183000 E, 82500 N. This is because a higher resistivity of above 20 Ohm.m but below 30 Ohm.m this was deduced as a steam cap on a porous medium. The steam cap deduction was based on the fact that an up domed resistivity structure at depth was inferred to have a high temperature; a higher resistivity above a clay mineral resistivity level (10 Ohm.m) could be a material that is not liquid but gaseous. Three dimensional inversion of resistivity data has proved to be a superior geophysical method of exploration with respect to other lower dimensional inversions. The clarity of the results obtained clearly signify that the method can significantly unearth geothermal structures and aid effective exploration for the resource.

5.2 Recommendations

Some more MT sounding are required to the North East of the prospect. This data might refine the model in the North East of the prospect. The researcher recommends a conceptual model taking into account the recovered model 3D resistivity model for future geothermal prospecting in Korosi geothermal prospect. Taking into account that there is not geophysical method that can stand alone but all complement each other to achieve an all-inclusive geothermal conceptual model, the researcher recommends that other geo-scientific like geology and geochemistry can be incorporated to conclude on the real size of the geothermal reservoir.

5.3 Research Contributions

Theoretically the assumptions involved in the lower dimensional interpretation of the electrical resistivity restrict the conductivity from varying in different directions as it should naturally. These assumptions underscores the use of higher dimensional interpretation especially for geothermal research.

Practically this research has great contributions such that during the entire process of the data preparations and inversions, the researcher is in control of the back end processes as well as feeding in the required data from the interface. The researcher is in contact with what is happening during the entire process as opposed to the lower dimensional inversion codes which allows only uploading data and only gives results with back end processes completely concealed thus reducing researcher controls and contact with the program.

5.4 Future Comments

On all future works, dimensionality analysis is recommended before an expensive 3D inversion is undertaken. This will establish whether or not the 3D inversion is required. Quite often 3D inversion will be required for geothermal exploration. This is qualified by the fact that the conductivity varies in all directions in a geothermal environment thus 3D interpretation is recommended in all future geothermal explorations. This recommendation is anchored to the fact that there is better clarity of imagery recovered from 3D inversion models than any lower dimensional interpretation.

REFERENCES

Árnason, K. (1989). Central loop transient electromagnetic soundings over a horizontally layered earth. *Orkustofnun.*

Árnason, K. (2008). The Magneto-telluric static shift problem. Iceland GeoSurvey - *ISOR, report, ISOR08088, 17 pp.*

Árnason, K. E. (2010). Joint 1-D inversion of TEM and MT data and 3-D inversion of MT data in the Hengillarea, SW Iceland. *Geothermics*, Vol 39, Issue 1, 13–34.

Arthur, M. M. (2016). Three dimensional inversions of mt resistivity data to image geothermal systems: case study, korosi geothermal prospect. *African Rift Geothermal Conference (ArGeo C6)*.

Arthur, M. M. (2016). Three dimensional inversions of mt resistivity data to image geothermal systems: Case study, Korosi geothermal prospect. Unpublished, Thesis research Progress Works.

Avdeev, D. B. (2002). Three-dimensional induction logging problems, Part I: An integral equation solution and model comparisons. *Geophysics*, Volume 67, Issue 2, Pages 413-426.

Bahr, K. (1988). Interpretation of the magnetotelluric impedance tensor: regional induction and local telluric distortion. *J. Geophys*, Volume 62, Issue 2, pages 119-127.

Cumming, W. M. (25-29 April 2010). Resistivity Imaging of Geothermal Resources Using 1D, 2D and 3D MT Inversion and TDEM Static Shift Correction Illustrated by a Glass Mountain Case History. *World Geothermal Congress* (pp. Pages 1-10). Bali, Indonesia: World Geothermal Congress 2010.

deGroot-Hedlin, C. (1991). Removal of static shift in two dimensions by regularized inversion. *Geophysics*, Volume 56;Issue 12, Pages 2102-2106.

deGroot-Hedlin, C. C. (1990.). Occam's inversion to generate smooth, two-dimensional models from magnetotelluric data. *Geophysics*, Volume 55, Issue 12, Pages 1613–1624.

deGroot-Hedlin, C., & Constable, S. (1990). Occam's inversion to generate smooth, two-dimensional models from magnetotelluric data. *Geophysics*, Vol 55, Issue 12 , 1613-1624.

Gichira, J. (2012). Joint 1D inversion of MT and TEM data from Menengai geothermal field, Kenya. 1670-7427.

Hersir, G. P. (1991). Geophysical exploration for geothermal resources: principles and application. *Orkustofnun.*

Jiracek, G. R. (1990). Near-surface and topographic distortions in electromagnetic induction. *Surveys in Geophysics*, Volume 11, Issue 2-3, Pages 163-203.

Jones, A. (1988:). Static shift of magnetotelluric data and its removal in a sedimentary basin environment. *Geophysics, 53-7,*, Volume 53, Issue 7, Pages 967-978.

Jones, A. G. (1988). Static shift of magnetotelluric data and its removal in a sedimentary basin environment. *Geophysics*, Volume 53,Issue 7, Pages 967-978.

Lichoro, C. M. (2014). Geophysical prospecting of Korosi Geothermal prospect. Nakuru: Unpublished GDC internal report for Well Pegging.

Mackie, R. L. (1994). Three-dimensional electromagnetic modeling using finite difference equations: the magnetotelluric example. *Radio Science*, Volume 29, Issue 04, Pages 923–935.

Mariita, N. (2006). Integration of Geophysical data from Korosi geothermal prospect. Website material.

Meju, Y. S. (2006). Three-dimensional joint inversion for magnetotelluric resistivity and static shift distributions in complex media. *Journal of geophysical research*, VOL. 111, B05101, doi:10.1029/2005JB004009.

Muturia Lichoro, C. (2013). Multi-dimensional interpretation of electromagnetic data from Silali geothermal field in Kenya: Comparison of 1-D, 2-D and 3-D MT inversion. Orkustofnun, Grensásvegur 9, Number 4 IS-108 Reykjavík, Iceland.

Newman, G. A. (2000.). Three-dimensional magnetotelluric inversion using non-linear conjugate gradients. *Geophysical journal international*, Voume 140, Issue 2, Pages 410–424.

Ogawa, Y. U. (1996). A two-dimensional magnetotelluric inversion assuming Gaussian static shift. *Geophysical Journal International*, Volume 126, Issue 1, Pages 69-76.

Pellerin, L. G. (1990). Transient electromagnetic inversion: A remedy for magnetotelluric static shifts. *Geophysics*, Volume 55,Issue 9, Pages 1242-1250.

Phoenix,Geophysics. (2005). Data processing user guide. Toronto, USA: Phoenix Geophysics Limited.

Raymond, G. N. (2011). Geophysical investigation of Korosi-Chepchuk Geothermal Prosepect. Nakuru: Unpublished, GDC internal report.

Sasaki, T. U. (2006). Stable 3D inversion of MT data and its application to. *Exploration Geophysics*, vol 37, Issue 3, pages 223–230.

Silas M. Simiyu. (April 2010). Status of Geothermal Exploration in Kenya and Future Plans for Its Development. *Proceedings World Geothermal Congress*, (pp. 25-29). Bali, Indonesia,.

Siripunvaraporn, W. (2006). WSINV3DMT version 1.0.0 or Single Processor Machine. THAILAND, Bangkok 10400, Rama 6 Rd., Rachatawee,.

Siripunvaraporn, W. E. (2000). An efficient data-subspace inversion method for 2-D magnetotelluric data. *Geophysics*, Volume 65, Issue 3, 791-803.

Siripunvaraporn, W. E. (2002). Numerical accuracy of magnetotelluric modeling: a comparison of finite difference approximations. *Earth, planets and space*, Volume 54, Issue 6, Pages 721-725.

Siripunvaraporn, W. E. (2005). Three-dimensional magnetotelluric inversion: data-space method. *Physics of the Earth and planetary interiors*, Volume 14o, Issue 1, Pages 3-14.

Siripunvaraporn, W. E. (n.d.). An efficient data-subspace inversion method for 2-D magnetotelluric data. *Geophysics*, Vol 65, Issue 3, Pages 791-803.

Smith, J. T. (1996.). Conservative modeling of 3D electromagnetic fields. Part II. Biconjugate gradient solution and an accelerator. *Geophysics*, Volume 61, Issue 5, Pages 1319–1324.

Sternberg, B. J. (1988:). Correction for the static shift in magnetotellurics using transient electromagnetic soundings. *Geophysics, 53,*, Volume 53, Issue 11, Pages 1459-1468.

Toshihiro Uchida*, T. J.-R., & Yutaka Sasaki, K. (2001). Three-dimensional inversion of magnetotelluric data at the Bajawa geothermal field, eastern.

Uchida, T., Lee, T. J., Sasaki, Y., Honda, M., & Andan, A. a. (September 9-14, 2001). *Three-dimensional inversion of magnetotelluric data at the Bajawa geothermal field, eastern.* San Antonio, Texas.

Weerachai Siripunvarapron, G. E. (2006). WSINV3DMT version 1.0.0 for Single Processor Machine, User Manual. Bangkok: Thailand research Fund.

Zhang, J. (1987). Increased synthesis of ABA in partially dehydrated root tips and ABA transport from roots to leaves. *Journal of Experimental Botany*, Volume 38, Issue 12, pages 2015-2023.

APPENDIXES

MT data.

This section presents the quality of MT data that was the input to the model. It is evident that the data used was on average of good quality as revealed from the curves in this section. A few curves of resistivity vs frequency and phase vs frequency are shown. Inconsistency of the

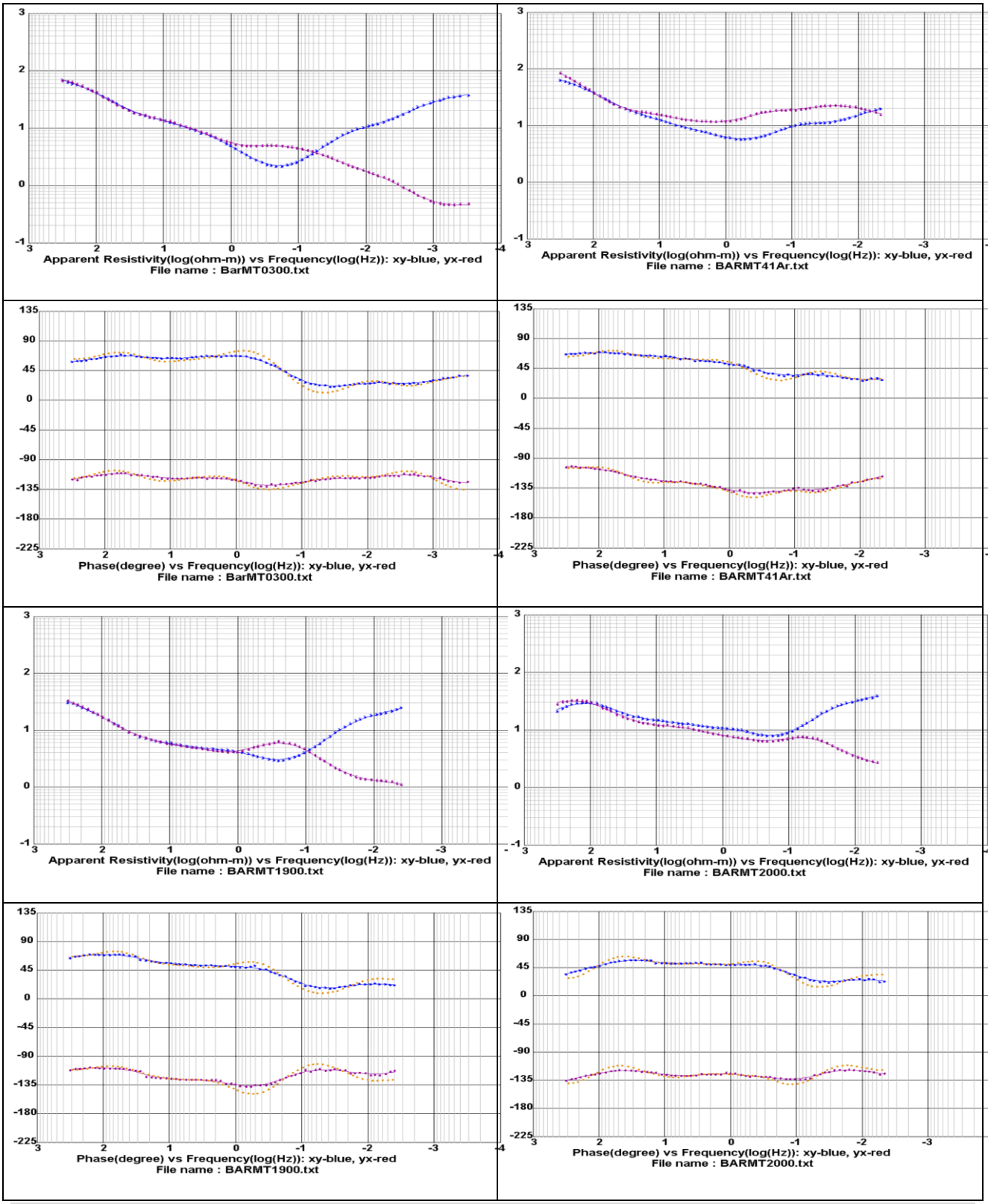

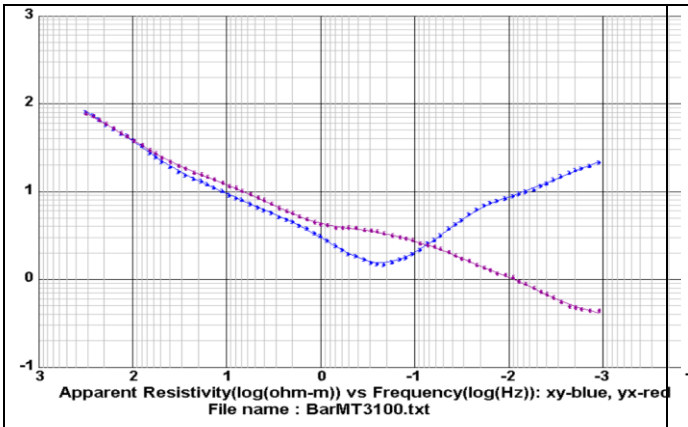
Apparent Resistivity(log(ohm-m)) vs Frequency(log(Hz)): xy-blue, yx-red
File name : BarMT3100.txt

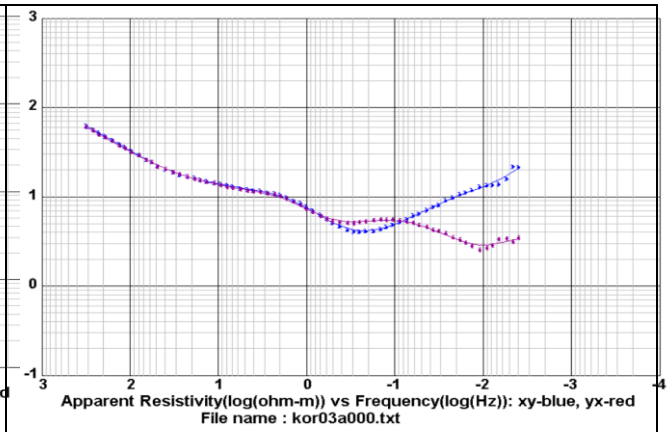
Apparent Resistivity(log(ohm-m)) vs Frequency(log(Hz)): xy-blue, yx-red
File name : kor03a000.txt

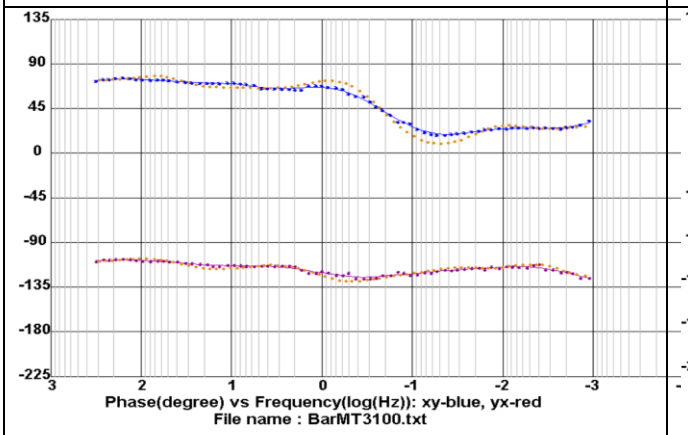
Phase(degree) vs Frequency(log(Hz)): xy-blue, yx-red
File name : BarMT3100.txt

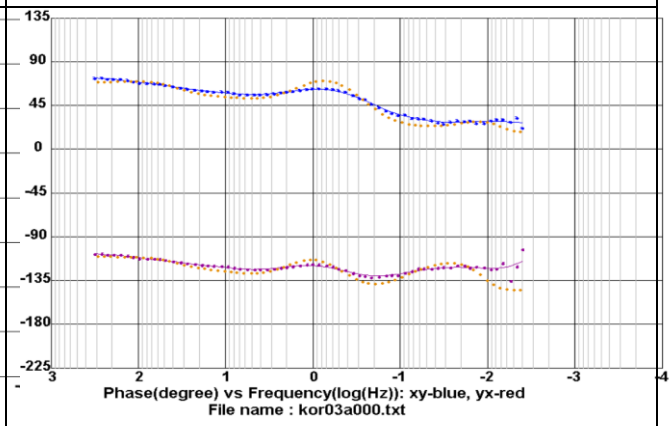
Phase(degree) vs Frequency(log(Hz)): xy-blue, yx-red
File name : kor03a000.txt

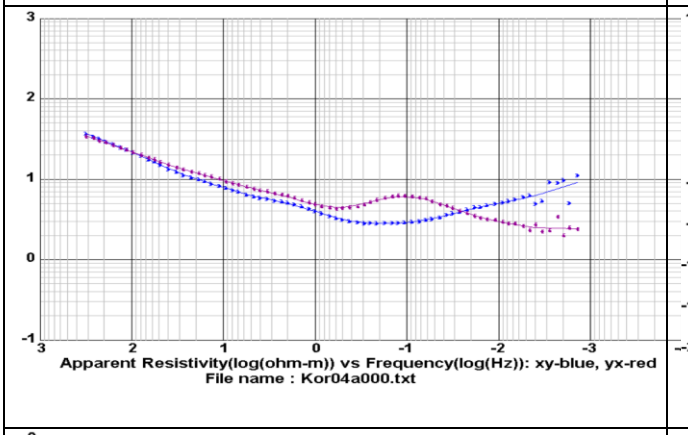
Apparent Resistivity(log(ohm-m)) vs Frequency(log(Hz)): xy-blue, yx-red
File name : Kor04a000.txt

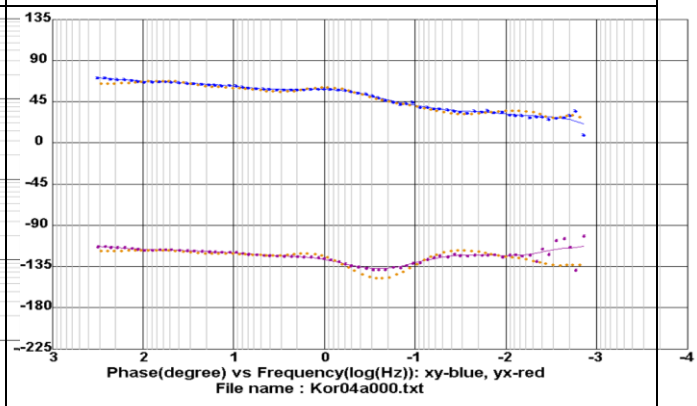
Phase(degree) vs Frequency(log(Hz)): xy-blue, yx-red
File name : Kor04a000.txt

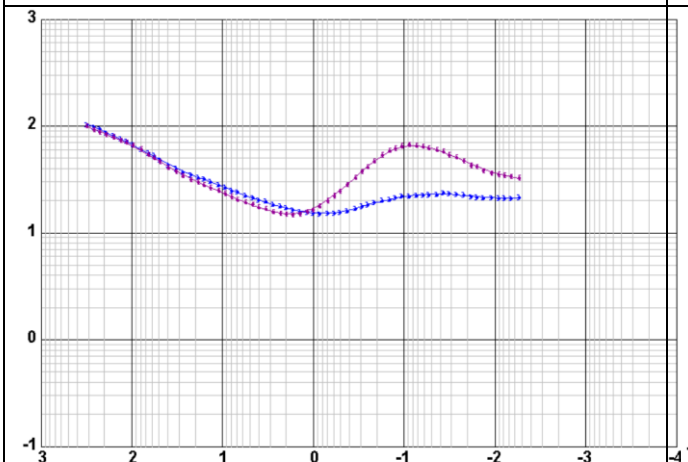
Apparent Resistivity(log(ohm-m)) vs Frequency(log(Hz)): xy-blue, yx-red
File name : kor05a000.txt

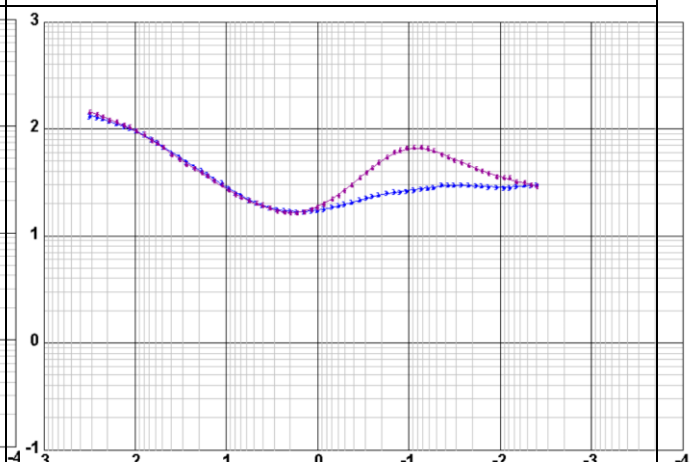
Apparent Resistivity(log(ohm-m)) vs Frequency(log(Hz)): xy-blue, yx-red
File name : kor06a000.txt

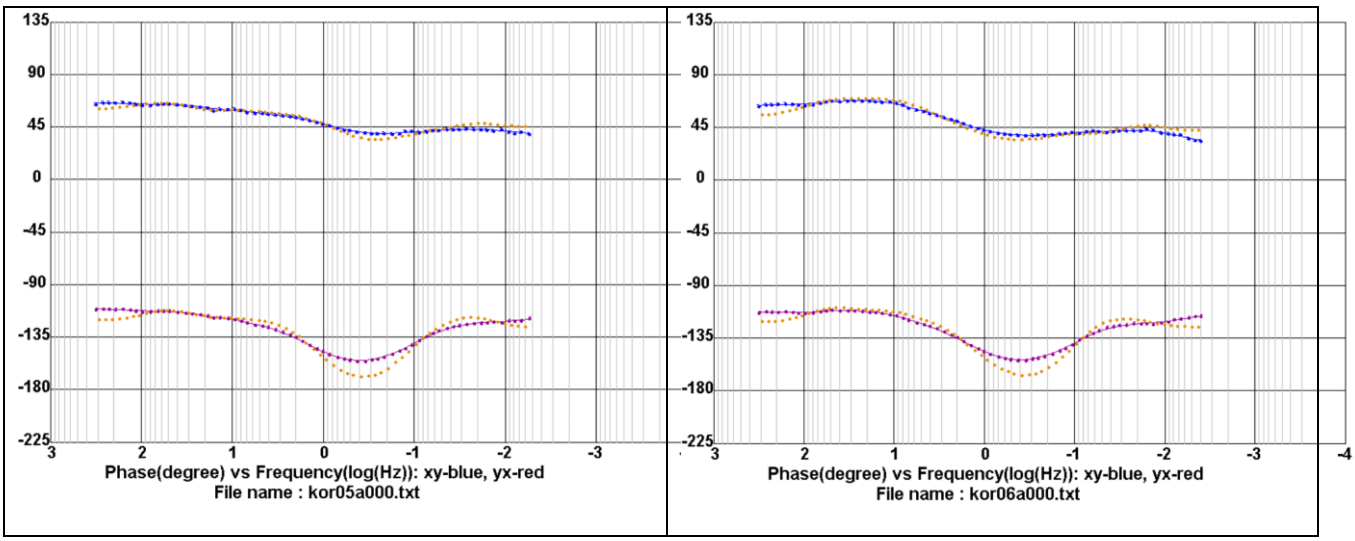
135
90
45
0
-45
-90
-135
-180
-225
3
2
1
0
-1
-2
-3
Phase(degree) vs Frequency(log(Hz)): xy-blue, yx-red
File name : kor05a000.txt
135
90
45
0
-45
-90
-135
-180
-225
3
2
1
0
-1
-2
-3
-4
Phase(degree) vs Frequency(log(Hz)): xy-blue, yx-red
File name : kor06a000.txt